THE EFFECT OF JET ENTRAINMENT ON LIFT AND MOMENT FOR A THIN AEROFOIL WITH BLOWING

by

I. Wygnanski and B.G. Newman

Report 63-1

Mechanical Engineering Research Laboratories

McGill University

Supported under D.R.B. Grant Number 9551-12

Montreal June 1963

SUMMARY

Jet-flap theory for thin aerofoils has been extended to include the effect of jet entrainment on the external flow when the jet is blown over the upper surface of the aerofoil. The effective camber of the aerofoil is increased by the sink effect due to entrainment and the increase of lift at zero incidence is proportional to the square root of the jet momentum coefficient. Formulae and charts are presented to facilitate the determination of the increments of lift and pitching moment due to this effect. The theory is shown to be in first-order agreement with the exact solution for a circular-arc aerofoil of small camber.

The new theory is compared with four old sets and one new set of experimental data. It greatly improves the accuracy of prediction for cases where the incidence and flap angle are small. The new theory substantiates the usefulness of a small flap in applications of the jet flap principle.

NOTATION

a - radius of transformation circle and one quarter of the aerofoil chord

A_ℓ - coefficients in thin aerofoil theory (equation 2.21)

b - width of the blowing slot

C_J - jet-momentum coefficient $= \dfrac{J}{\frac{1}{2}\rho U_\infty^2 (4a)}$

C_L - lift coefficient $= \dfrac{L}{\frac{1}{2}\rho U_\infty^2 (4a)}$

C_{M_o} - nose-up moment coefficient about the mid chord $= \dfrac{M_o}{\frac{1}{2}\rho U_\infty^2 (4a)^2}$

E - elliptic integral of the second kind

F - elliptic integral of the first kind

h - height of a control volume embracing the jet

i - $\sqrt{-1}$

$I_{1,2,3,4}$ functions of λ and $\dfrac{S_o}{4a}$

J - jet momentum per unit span

ℓ - mixing length for momentum transfer

L - lift per unit span

M_o - nose-up pitching moment per unit span about the mid-chord part

Q_n - strength of the n^{th} sink

q - volume flux in the wall jet per unit span

R - 'real part of'

r - radius of curvature of the centre-line of the jet

S - distance measured along the axis of the jet and downstream of the slot

S_o - distance of the slot downstream of the hypothetical origin of the jet

U - mean velocity in the jet

U_m - maximum velocity in the jet

U_1 - local mean velocity in the free stream

U_∞ - free stream velocity

W - complex potential function

x - real axis in the physical complex plane

y - distance measured perpendicular to the jet, or the imaginary axis in the physical complex plane

$z = x + iy$

α - angle of attack of the aerofoil

β - twice the camber ratio for a thin circular arc aerofoil

γ - circulation per unit length of camber line

Γ - total circulation round the aerofoil

δ^* - boundary layer displacement thickness

δ - total thickness of the wall jet

ϵ - turbulent eddy viscosity

$\zeta = \xi + i\eta$
$\zeta' = \xi' + i\eta$
} coordinate systems in the complex circle plane.

λ - identifies the proportion of the chord from the leading edge at which the slot is located

θ - angle through which a wall jet is turned over a convex surface

ρ - density of the fluid

σ - growth parameter determining the rate of growth of the jet

τ - angle between the axis of the jet and the chord of the aerofoil at the trailing edge

Φ - polar angle in the ζ' plane

χ - polar angle in the ζ plane

ψ - stream function

Suffix n identifies the position of the n^{th} sink Q_n

1. INTRODUCTION

Blowing over the upper surface of a wing is a powerful means of increasing the usable lift coefficient and reducing the landing and take-off speeds of aircraft. Although the method usually requires more power than the corresponding use of suction (in particular distributed suction), it can yield higher lift coefficients and furthermore is a great deal easier to apply. The turbo-jet engine provides the required high-pressure air, and the ducts which convey it to the blowing slot can be relatively small. A number of aircraft use this form of lift augmentation. For example on the American Lockheed F104 Starfighter blowing is applied to the trailing-edge flaps, on the French Dassault Etenard IVM to both leading-edge and trailing-edge flaps and on the British Blackburn NA39 Buccanneer to leading and trailing-edge flaps and as well as the tailplane.

In the application of blowing a distinction is made between boundary-layer control and circulation control. The first function of the jet as it blows over the surface is to increase the mean kinetic energy of the fluid within the boundary layer so that the latter may advance without separation into a region of rising pressure e.g. over the upper surface of the wing near the leading edge or over a deflected trailing-edge flap. If the jet momentum is

sufficient the ideal lift coefficient corresponding to potential flow is obtained, although for large flap angles this occurs at a somewhat higher jet momentum than that required merely to prevent separation. In this regime of boundary-layer control the lift increment is roughly proportional to the first power of the jet momentum. A further increase of jet momentum produces an augmentation of lift which is roughly proportional to the square root of the jet momentum. This is the regime of circulation control or supercirculation and the jet leaves the trailing -edge with sufficient downward momentum to appreciably increase the circulation round the wing, as well as itself providing a direct contribution to the lift from the component of the jet momentum. Indeed circulation control alone may be obtained by blowing the jet obliquely from the trailing edge of the wing, as in the jet flap. Experiments indicate however, that there is a substantial gain in lift when the jet is blown over a suitably-deflected physical flap.(1)

A number of theoretical methods have been developed for predicting the increment of lift and moment due to supercirculation round aerofoils. Stratford attempted to calculate the lift by assuming that the jet flap was equivalent to a physical flap.(2) More realistic assumptions were made by Helmbold (3), Spence(4), Legendre(5) and Woods(6) who replaced the jet by a vortex sheet springing from the trailing edge. Woods obtained solutions using the hodograph

method while Spence and Malavard[7] linearized the problem assuming small incidence and jet deflection. Spence obtained numerical solutions analytically, while Malavard used the rheoelectric analogy for potential flow. In general it appears that these linearized solutions give useful results even up to quite large jet-flap deflections.

In all these theories the mixing of the jet with the main stream is neglected. In reality the jet continually entrains fluid from the main stream. This is apparent in the smoke tunnel pictures of the flow past a thin aerofoil with blowing at 50% chord which are shown in Fig.1. It is clear that the entrainment increases the effective camber of the aerofoil and that the detailed effect could be represented in a potential flow theory by placing a suitable distribution of sinks on the upper surface of the aerofoil downstream of the blowing slot. In this way the stream functions for a great variety of free jet flows have been given by Taylor.[8] Furthermore within the context of linearized theory it is clear that the entrainment which takes place on both sides of the jet downstream of the trailing edge may be assumed to have no effect on the circulation. In the present paper therefore the effect of such a distribution of sinks, which extend from an arbitrary slot position to the trailing edge, is analyzed for a thin aerofoil. The purpose is to determine the lift and moment and to assess its magnitude in cases of practical importance.

A solution is first obtained for a circular-arc aerofoil of small camber by conformally transforming the flow round a circular cylinder. The lift and moment coefficients are determined. The solution for a thin aerofoil with arbitrary camber line is then obtained by extending classical thin-aerofoil theory. As a preliminary the distribution of circulation for a flat-plate aerofoil is obtained as a particular case of the solution for a circular-arc. The two theories are compared for the case of a circular-arc in order to assess the accuracy of the thin aerofoil theory. Formulae and graphs are presented which enable the lift and moment to be calculated for any thin aerofoil, jet momentum coefficient, slot position and slot thickness. The thin aerofoil theory is then compared with five sets of experimental data including a new set on an aerofoil with sharp leading edge. The comparison includes that of the streamline pattern for the thin aerofoil shown in Figure 1.

2. THEORY

2.1 The Distribution of Sinks which Represent the Entrainment Effect of a Wall Jet on an External, Irrotational Flow.

The mean velocity distribution in an incompressible free jet is given with sufficient accuracy by assuming that the turbulent eddy viscosity ϵ is constant across the flow. (Görtler[9])

$$U = \frac{3J\sigma}{4\rho(S+S_o)}^{\frac{1}{2}} \operatorname{sech}^2 \frac{\sigma y}{S+S_o} \qquad \ldots(2.1)$$

where S is the distance measured downstream from the slot

S_o is the distance of the slot downstream of the hypothetical origin, where a jet of momentum J emerging from an infinitesimally thin slot ($b \to 0$) would produce the same flow.

y is the distance from the centre line of the jet

σ is an empirical constant which is determined from measurements of the growth of the jet and is of order 10.

A value of S_o may be obtained by equating the volume flow from the slot, neglecting internal boundary layers, to the mass flow in the hypothetical jet.[10] On this basis $S_o = \frac{\sigma b}{3}$

Following Carriere and Eichelbrenner[11] the mean velocity profile for a turbulent wall jet in streaming flow may be approximated by superposing half a free jet on a turbulent boundary layer of thickness δ, equal to that of the wall jet. (Figure 2.1)

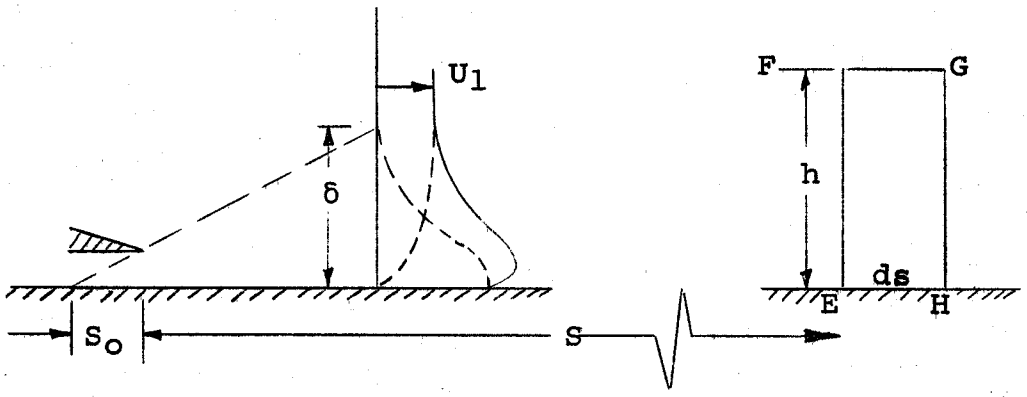

Figure 2.1

Consider the control volume EFGH of width ds and height h ($>\delta$) situated at distance s from the slot. Using equation (2.1) the volume flux q entering across EF is

$$q = \left[\frac{3J(S+S_o)}{2\rho\sigma}\right]^{\frac{1}{2}} + U_1\ (h-\delta^*) \qquad \ldots(2.2)$$

where U_1 is the free stream velocity and δ^* is the displacement thickness of the boundary-layer component of the wall-jet profile.

The flux leaving the control volume across GH is $q + \frac{dq}{ds}\,ds$ and thus $\frac{dq}{ds}\,ds$ is the volume flux entering across FG

where $$\frac{dq}{ds} = \left[\frac{3J}{8\rho\sigma(S+S_o)}\right]^{\frac{1}{2}} + \frac{d}{ds}\left[U_1(h-\delta^*)\right] \qquad \ldots(2.3)$$

If the wall jet were absent and the flow were inviscid $\frac{dq}{ds}$ would be $\frac{d}{ds}(U_1\ h)$. Thus the difference is the volume flux which can be attributed to jet entrainment and its effect on the external flow can be simulated by a sink strength

$\left(\frac{dq}{ds}\right)_{entr.}$ per unit length of wall,

$$\left(\frac{dq}{ds}\right)_{entr.} = \left[\frac{3a}{4\sigma(S+S_o)}\, C_J\right]^{\frac{1}{2}} - \frac{d}{ds}(U_1\, \delta^*) \quad \ldots(2.4)$$

where C_J is the jet momentum coefficient based on an aerofoil chord 4a and $= \frac{J}{\frac{1}{2}\rho U_\infty{}^2(4a)}$

If the inner-wall boundary layer thickness is small compared with the thickness of the jet the second term in equation (2.4) can usually be neglected for moderate to large values of C_J and the equation simplifies to

$$\left(\frac{dq}{ds}\right)_{entr.} = \left[\frac{3a}{4\sigma(S+S_o)}\, C_J\right]^{\frac{1}{2}} \quad \ldots(2.5)$$

The word 'entrainment' is used here to denote the total effect which the jet produces on the external flow. It is an appropriate term in the context of the above approximation since the outflow associated with the blockage effect of the wall jet has been neglected compared with the inflow associated with the entrainment of vortical fluid at the edge of the turbulent shear flow.

2.1.1 The Growth Parameter σ

To apply equation (2.5) an appropriate value of σ must be chosen. It is clear from equation 2.1 that the rate of spread of the jet is inversely proportional to σ.[9, 10]

The variation of σ due to jet curvature, wall proximity and so on, can be qualitatively explained if the turbulent eddy viscosity , which is assumed to be constant across the flow in deriving equation (2.1), is equated to $\ell^2\left|\frac{dU}{dy}\right|$ where ℓ is the mixing length for momentum transfer. On this basis $\sigma \sim \frac{\delta^2}{\ell^2}\ \frac{U_m}{U_m - U_1}$ where U_m is the maximum velocity in the jet.[10]

For a two dimensional incompressible free jet the measurements of Reichardt[12], Forthmann[13] and Knystautas[14] indicate that at distances greater than 5 slot widths downstream of the slot, equation (2.1) is a good representation of the mean velocity profile when $\sigma = 7.7$.

(i) <u>Effect of Compressibility</u>

Experimental evidence for reattaching jets indicates that the rate of spread of a two-dimensional turbulent jet is reduced by compressibility.[15] This is consistent with the Libby and Ting's[16] use of Mager's[17] transformation which leads to the assumption that the turbulent eddy viscosity ϵ is proportional to ρ^{-2} and hence decreases with increasing jet density. Moreover since ϵ varies across the jet the mean velocity can no longer be represented strictly by the simple equation (2.1). However for the present purposes it is proposed to assume that equation (2.1) still applies using a suitable average value for σ. The work on free

mixing layers provides information on the appropriate choice of σ. For an incompressible free mixing layer, theory[18] assuming a constant eddy viscosity across the flow gives good agreement with experiment when σ is approximately 12. At a Mach number of 0.7 Lawrence's experimental results are in agreement with Crane's[19] analysis assuming a constant eddy viscosity across the flow, where $\sigma = 12.7$, and at a Mach number of 1.4 the measurements of Johannesen give $\sigma = 21.9$. Similar analyses by Pai and Abramovich[18] are in agreement with experiment at a Mach number of 1.6 when $\sigma = 17$. It is concluded therefore that σ is approximately constant at subsonic speeds but should be increased by a factor of approximately two at low supersonic speeds.

(ii) Effect of Wall Proximity

The outer part of a fully developed incompressible turbulent wall jet [20, 21, 22] has a velocity distribution which is similar to that of half a free jet and equation 2.1 fits it satisfactorily with σ approximately 13. Thus a wall jet entrains external fluid less rapidly and this is attributed to a reduction in the lateral scale of the turbulence and the mixing length l due to the constraint of the wall.

(iii) Effect of an External Stream

Since $\sigma \sim \frac{U_m}{U_m - U_1}$ for a given $\frac{\delta}{\ell}$ it is anticipated that σ will increase with $\frac{U_1}{U_m}$.

The assumption of a constant value of σ for a given flow is of course only valid if the jet is flowing in a particular pressure distribution which maintains $\frac{U_m}{U_1}$ constant and renders it self-preserving.[23] Measurements by Patel[22] on self-preserving wall jets in streaming flow confirm that the appropriate value of σ increases with $\frac{U_1}{U_m}$. Patel's results are summarized in Figure 2.

(iv) Effect of Curvature

In a curved jet the rate of entrainment is increased on the convex side of the jet and decreased on the concave side. This can be attributed to the change in average transverse movement of a fluid particle associated with the unbalanced centrifugal acceleration in each case.[10] For example random movement of a fluid particle towards the convex side of the jet brings fluid of high velocity into a region where the lateral pressure gradient is insufficient for equilibrium and hence the fluid travels further before mixing with its surroundings. Formulae for the associated change of mixing length have been proposed by Sawyer[24] and Stratford[25]. An empirical formula

given by Newman for the rate of growth of a wall jet round the outside of a circular cylinder gives

$$\sigma = C_1 - C_2\theta \qquad \ldots(2.6)$$

where θ is the angle through which the jet is turned round a convex surface and is measured from the hypothetical origin. The most accurate measurements to date have been made by Fekete[26] and give $C_1 = 9.6$, $C_2 = 2.14$ at high R_e.

2.1.2 The Jet Momentum Coefficient C_J

As the wall jet flows over the aerofoil, the jet momentum decreases due to the skin friction at the wall and also due to possible convex curvature of the surface.[10] However the decrease is usually small and unimportant for moderate-to-large values of C_J and for small flap deflections and incidence. Thus for the purpose of determining the sink effect due to jet entrainment using equation (2.5), it is usually sufficiently accurate to take the jet momentum as that leaving the slot.

The prediction of the lift and moment on an aerofoil using ideal fluid theory is not straightforward when the jet blows over a flap and leaves the trailing edge at an appreciable angle to the free stream. The theory incorporating sink effect which is given in sections 2.2 may be added to Spence's jet flap theory for thin aerofoils[4, 27, 28], but the appropriate value of C_J and the average angle τ at which the jet leaves the trailing

edge are to some extent uncertain. In French experiments[1] it is customary to determine these values from wind-off measurements of the mass flow of fluid being ejected, together with the nett thrust on the jet, which is obtained by subtracting the integrated pressure force on the outside of the model from the total force on the model. Alternatively the momentum of the flow at the trailing edge may be determined theoretically by using one of the empirical methods for the development of a wall jet in any pressure gradient, (Carriere and Eichelbrenner[11] or Thomas[29]). A third alternative, which gives the appropriate value of C_J only, is to use one of the empirical curves presented by Williams[30] and Thomas[29] to determine the value of C_J required to prevent separation and then to use the excess amount of C_J as the appropriate value for insertion in the jet-flap theory.

2.2 The Effect of the Sinks on the Flow round an Aerofoil and the Calculation of Lift and Moment.

The analysis will be confined to thin aerofoils of small camber and at small incidence. Flap deflections, if any, are assumed to be small.

As the wall-jet proceeds over the upper surface of the aerofoil it entrains the surrounding irrotational flow. Thus the downwash velocity near the upper surface is increased, and hence the overall circulation round the aerofoil (Figure 1). Downstream of the trailing edge however, entrainment occurs on both sides of the jet and,

if the angle which the jet makes with the free stream velocity is small, there will be no nett additional downwash due to entrainment. For the purpose of analyzing this effect therefore, the jet is replaced by a series of sinks on the upper surface and these extend from the slot to the trailing edge. The strength of the sinks is given by equation 2.5.

Spence's thin aerofoil theory for jet flap effect without entrainment is subsequently superimposed to give the total lift and moment on a thin aerofoil with blowing.

2.2.1 Lift and Moment for a Circular-Arc Aerofoil with Sinks Distributed over its Upper Surface.

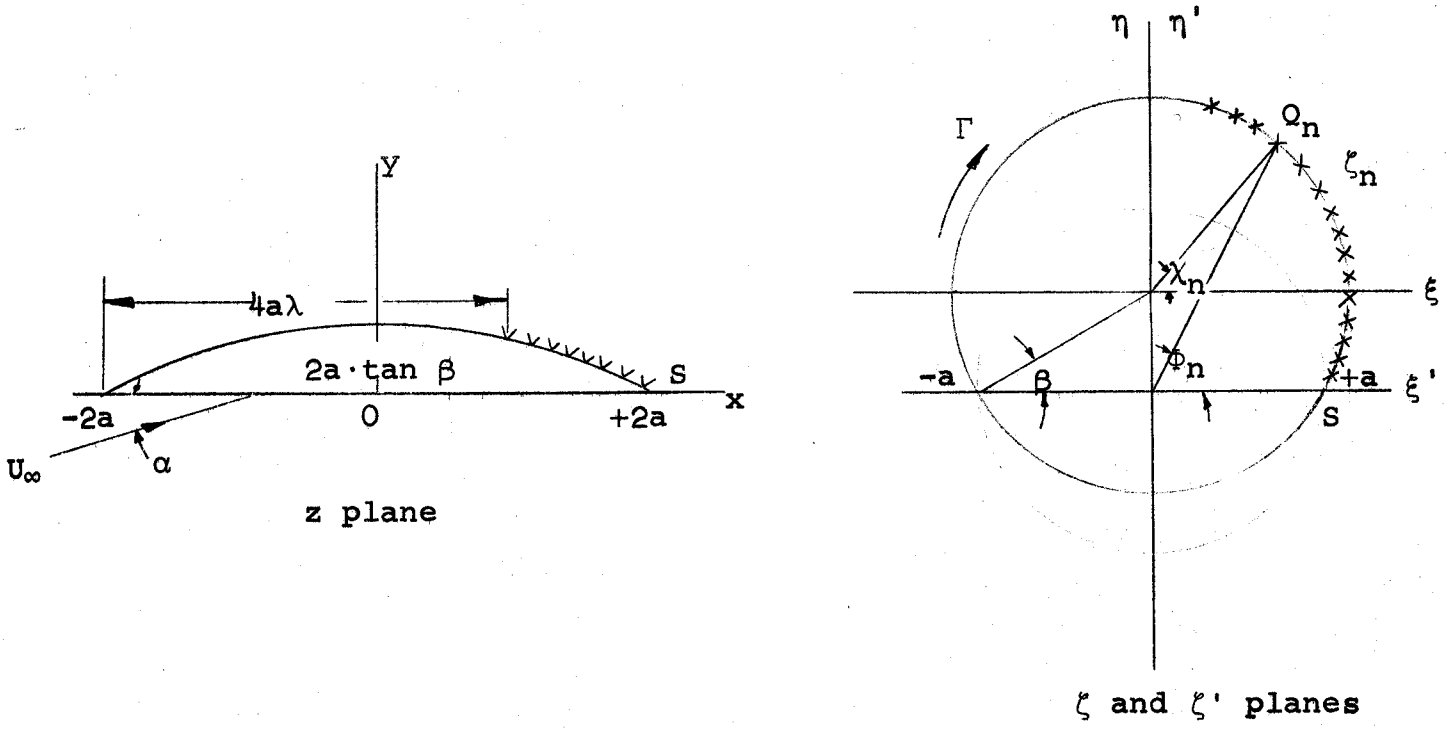

Figure 2.2

Consider a circular-arc aerofoil of chord 4a and camber ratio $\frac{1}{2}\tan\beta$. This is placed at an incidence α in an irrotational flow of velocity U_∞.

The blowing slot is located λ of the chord from the leading edge, so that the sinks extend from $x = 4a\lambda - 2a$ to $x = 2a$ on the upper surface.

The circular-arc is transformed into a circle of radius $a\sec\beta$ in the ζ' plane by the Joukowski transformation

$$z = \zeta' + \frac{a^2}{\zeta'} \qquad \ldots(2.7)$$

The transformation is made single-valued by considering the flow outside the circle only. However in order to keep the circle a streamline an image of each sink is added at the inverse point and a source of the same strength is added at the centre of the circle. In this case the sinks and their images obviously coincide on the circumference of the circle. The strength of each sink is unaltered by transformation.(31)

To facilitate the analysis a further linear transformation is introduced

$$\zeta = \zeta' - ia\tan\beta \qquad \ldots(2.8)$$

The complex potential for the flow about the circle with circulation Γ is:

$$W(\zeta) = U_\infty\left(e^{-i\alpha}\zeta + \frac{a^2\sec^2\beta}{\zeta e^{-i\alpha}}\right) + \frac{i\Gamma}{2\pi}\ln\zeta + \sum_{n=1}^{n=N}\frac{Q_n}{2\pi}\left[\ln\zeta - 2\cdot\ln(\zeta-\zeta_n)\right] \qquad \ldots(2.9)$$

where Q_n is the strength of n^{th} sink located at ζ_n and there are N sinks altogether.

The complex conjugate velocity in the physical z plane

$$\frac{dW}{dz} = \frac{dW}{d\zeta} \cdot \frac{d\zeta}{d\zeta'} \cdot \frac{d\zeta'}{dz}$$

$$= \left[U_\infty\left(e^{-i\alpha} - \frac{a^2\sec^2\beta}{\zeta^2 e^{-i\alpha}}\right) + \frac{i\Gamma}{2\pi\zeta} + \sum_1^N \frac{Q_n}{2\pi}\left(\frac{1}{\zeta} - \frac{2}{\zeta-\zeta_n}\right)\right]\left[1 - \frac{a^2}{\zeta'^2}\right]^{-1} \quad \ldots(2.10)$$

Applying the Kutta condition, S is a stagnation point i.e.

$$\frac{dW}{dz} = 0 \text{ at } \zeta = a \sec\beta\, e^{-i\beta}.$$

Putting $\zeta_n = a \sec\beta\, e^{-i\chi_n}$,

$$\Gamma = 4\pi a U_\infty \sec\beta \sin(\alpha+\beta) + \sum_1^N Q_n \cot\left(\frac{\chi_n+\beta}{2}\right) \quad \ldots(2.11)$$

Thus for small α and β (neglecting α^2 and β^2 compared with unity) the lift coefficient

$$C_L = \frac{\rho U_\infty \Gamma}{\frac{1}{2}\rho U_\infty^2 . 4a} = 2\pi(\alpha+\beta) + \frac{1}{2aU_\infty}\sum_1^N Q_n \cot\left(\frac{\chi_n+\beta}{2}\right) \quad \ldots(2.12)$$

The nose-up pitching moment about the origin O is most easily calculated using Blasius' theorem

$$M_O = \frac{1}{2}\rho\, R \oint \left(\frac{dW}{dz}\right)^2 z\,dz$$

Expanding $\left(\frac{dW}{dz}\right)^2$ and $z\,dz$ in ascending powers of $\frac{1}{\zeta}$ for small

α and β, it may be shown that

$$M_o = \frac{1}{2}\rho U_\infty^2 (16a^2)\left\{\frac{\pi\alpha}{2} + \frac{1}{4aU_\infty}\sum_1^N Q_n\left[\frac{\Gamma}{4\pi aU_\infty} + \frac{\beta}{2} + \sin\chi_n - \alpha\cos\chi_n\right]\right\} \quad \ldots(2.14)$$

Substituting for Γ from equation 2.11, the nose-up pitching moment coefficient about the mid chord,

$$C_{M_o} = \frac{\pi\alpha}{2} + \frac{1}{4aU_\infty}\sum_1^N Q_n\left[\sin\chi_n - \alpha\cos\chi_n + \alpha + \frac{3\beta}{2} + \right.$$

$$\left. + \frac{1}{4\pi aU_\infty}\sum_1^N Q_n \cot\left(\frac{\chi_n+\beta}{2}\right)\right] \quad \ldots(2.15)$$

Equations (2.12) and (2.15) give the lift and moment once the required sink strength and distribution have been substituted from equation (2.5).

2.2.2 The Distribution of Circulation for a Flat-Plate Aerofoil.

As a preliminary to the extension of classical thin aerofoil theory for any thin cambered aerofoil with sinks, the distribution of circulation over a flat-plate aerofoil is obtained. For the flat plate aerofoil the analysis of the previous section applies with $\beta = 0$.

Thus $\zeta' = \zeta = ae^{i\Phi}$, say, on the circle

Hence $x = 2a\cos\Phi$ after transformation

If $x_n = 2a\cos\Phi_n$ identifies the position of sink Q_n, $\chi_n = \Phi_n$ in this case (see Figure 2.2)

From equation 2.10, the velocity u over the flat plate in the physical plane

$$u = \frac{dW}{dz} = U_\infty \left[1 + \alpha\left(\frac{1-\cos\Phi}{\sin\Phi}\right)\right] + \frac{1}{4\pi a \sin\Phi} \sum_1^N Q_n \left[\cot\frac{\Phi_n}{2} + \cot\left(\frac{\Phi-\Phi_n}{2}\right)\right] \quad \ldots(2.16)$$

Thus the circulation per unit length of plate at $x = 2a\cos\Phi$ is

$$\gamma = u_{upper} - u_{lower}$$

$$= U_\infty \left[\frac{2\alpha(1-\cos\Phi)}{\sin\Phi} + \frac{1}{2\pi a\, U_\infty \sin\Phi} \sum_1^N Q_n\left(\cot\frac{\Phi_n}{2} + \frac{\sin\Phi_n}{\cos\Phi_n - \cos\Phi}\right)\right] \quad \ldots(2.17)$$

It is noted that equation (2.17) correctly satisfies the Kutta condition at the trailing edge.

2.2.3 Thin Aerofoil Theory for a Cambered Aerofoil with Sinks Distributed over its Upper Surface.

The aerofoil is replaced by a vortex sheet on the camber line with sinks distributed over the upper surface downstream of the slot.

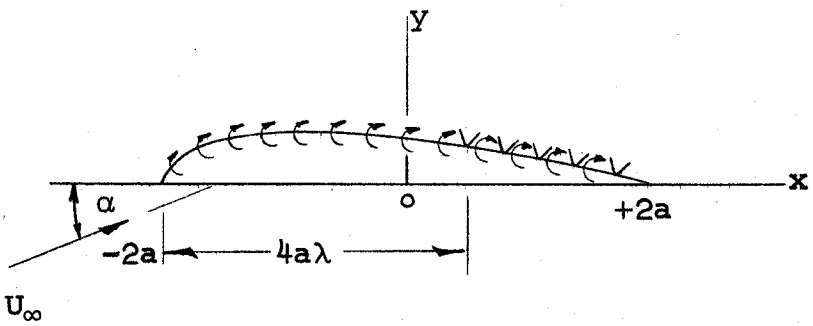

Figure 2.3

It is assumed that the velocity perturbations due to incidence, camber and sink effect are small compared with U_∞.

If γ is the circulation per unit length of camber line, the total circulation $\Gamma = \int_{-2a}^{+2a} \gamma dx$, if the camber is small. ...(2.18)

The upwash velocity $v(x)$ induced by the distributed vortices is

$$v(x) = \frac{1}{2\pi} \int_{-2a}^{+2a} \frac{\gamma dx'}{x' - x} \qquad ...(2.19)$$

and the aerofoil is a streamline if

$$\alpha + \frac{v}{U_\infty} = \frac{dy}{dx}, \text{ the slope of the camber line at } x. \qquad ...(2.20)$$

Equations (2.19) and (2.20), together with the Kutta condition are sufficient to determine the distribution of γ, and hence the lift and moment. To obtain the solution it is customary[32] to assume an expansion for γ as a Fourier series such that the Kutta condition is satisfied and such that the first term is compatable with the solution for the flat plate (equation (2.17)).
Thus it is assumed that

$$\frac{1}{2U_\infty}\gamma(\Phi) = A_o\left[\frac{1-\cos\Phi}{\sin\Phi} + \frac{1}{4\pi a U_\infty \alpha \sin\Phi}\sum_{n=1}^{N} Q_n\left(\cot\frac{\Phi_n}{2} + \frac{\sin\Phi_n}{\cos\Phi_n - \cos\Phi}\right)\right] +$$

$$+ \sum_{l=1}^{\infty} A_l \sin l\Phi \qquad ...(2.21)$$

The coefficients A are obtained in the usual way by substituting equation (2.21) in equations (2.19) and (2.20). This gives

$$\frac{dy}{dx} - \alpha = -A_o - \sum_{1}^{\infty} A_\ell \cos \ell\Phi \qquad \ldots(2.22)$$

since the integrals associated with the sink term vanish between the limits.(32)

Thus the conventional formulae for the Fourier coefficients are obtained

$$A_o = \alpha - \frac{1}{\pi} \int_{o}^{\pi} \frac{dy}{dx}\, d\Phi$$

$$A_\ell = -\frac{2}{\pi} \int_{o}^{\pi} \frac{dy}{dx}(\cos \ell\Phi)\, d\Phi \qquad \ldots(2.23)$$

From equation (2.18) the total lift

$$L = \rho U_\infty \int_{-2a}^{+2a} \gamma\, dx \qquad \ldots(2.24)$$

and

$$C_L = 2\pi \left[A_o\left(1 + \frac{1}{4\pi a U_\infty \alpha} \sum_{1}^{N} Q_n \cot\frac{\Phi_n}{2}\right) + \frac{A_1}{2} \right] \qquad \ldots(2.25)$$

From equation (2.5), the appropriate sink strength <u>per unit length</u> of jet is

$$U_\infty \left[\frac{3a}{4\sigma(S+S_o)} C_J \right]^{\frac{1}{2}}, \text{ where S is measured}$$

from the blowing slot.

The discrete sink distribution Q_n is therefore replaced by a continuous distribution of sinks. Thus if

the slot is situated at $4a\lambda$ from the leading edge of the aerofoil

$$S = 2a(1 + \cos\Phi_n) - 4a\lambda \qquad \ldots(2.26)$$

and the sink term in equation (2.25) may be written

$$\sum_1^N Q_n \cot\frac{\Phi_n}{2} = U_\infty\left[\frac{3aC_J}{4\sigma}\right]^{\frac{1}{2}} \int_{\text{Slot}}^{\text{Trailing Edge}} \frac{(\cot\frac{\Phi_n}{2})ds}{(S+S_o)^{1/2}}$$

$$= aU_\infty \left[\frac{3C_J}{\sigma}\right]^{\frac{1}{2}} \int_0^{\cos^{-1}(2\lambda-1)} \frac{(1+\cos\Phi_n)d\Phi_n}{(2\cos\Phi_n+2-4\lambda+\frac{S_o}{a})^{1/2}}$$

$$= 2aU_\infty \left[\frac{3C_J}{\sigma}\right]^{\frac{1}{2}} I_1 \qquad \ldots(2.27)$$

The integral I_1 may be solved in closed form,[33]

$$I_1 = \left\{ E\left[\bar{\theta},\ (1-\lambda+\frac{S_o}{4a})^{\frac{1}{2}}\right] - \frac{(1-\lambda+\frac{S_o}{4a})\sin\bar{\theta}\cos\bar{\theta}}{\sqrt{1-(1-\lambda+\frac{S_o}{4a})\sin^2\bar{\theta}}} \right\}_{\bar{\theta}_1}^{\frac{\pi}{2}}$$

$$\text{for } 1 > \lambda - \frac{S_o}{4a} > 0 \qquad \ldots(2.28)$$

where $\bar{\theta}_1 = \sin^{-1}\left[\frac{S_o}{4a\lambda(1-\lambda+\frac{S_o}{4a})}\right]^{\frac{1}{2}}$ and $S_o = \frac{2\sigma b}{3}$

E is a standard elliptic integral of the second kind, and is tabulated for example in references 34 and 35.

For the special case of $S_o = 0$ and $\lambda = 1$ equation (2.28) cannot be applied. However it is clear from equation (2.27) that $I_1 = 0$, as is the case for all values of S_o when $\lambda = 1$.

Equation (2.25) is therefore written

$$C_L = 2\pi \left\{ A_o \left[1 + \frac{1}{2\pi\alpha} \left(\frac{3C_J}{\sigma}\right)^{\frac{1}{2}} I_1 \right] + \frac{A_1}{2} \right\} \quad \ldots(2.29)$$

To facilitate the use of this equation I_1 is plotted against the slot location parameter λ for various values of $\frac{S_o}{4a}$ in Figure 3.

From Blasius' theorem, the moment about the origin for a flow consisting of a uniform stream inclined at α to the x axis upon which vortices and sinks are located, is

$$M_o = -\rho U_\infty \left(\sum_1^N Q_n x_n \alpha + \int_{-2a}^{+2a} \gamma x dx \right) + \frac{\rho}{2\pi} \sum_1^N Q_n \cdot \int_{-2a}^{+2a} \gamma dx \quad \ldots(2.30)$$

and $$C_{M_o} = \frac{M_o}{\frac{1}{2}\rho U_\infty^2 (4a)^2} = \frac{\pi A_o}{2} - \frac{\pi A_2}{4} +$$

$$+ \frac{1}{4aU_\infty} \sum_1^N Q_n \left[\frac{A_o}{\alpha} \sin\Phi_n - \alpha\cos\Phi_n + A_o + \frac{A_1}{2} + \frac{A_o}{4\pi a U_\infty \alpha} \sum_1^N Q_n \cot\frac{\Phi_n}{2} \right] \quad \ldots(2.31)$$

Once again replacing the discrete sink distribution by the continuous distribution from equation (2.5)

$$C_{M_o} = \frac{\pi A_o}{2} - \frac{\pi A_2}{4} + \frac{1}{4}\left(\frac{3C_J}{\sigma}\right)^{\frac{1}{2}}\left\{\frac{A_o}{\alpha} I_3 - \alpha I_2 + I_4\left[A_o + \frac{A_1}{2} + \frac{A_o}{2\pi\alpha}\left(\frac{3C_J}{\sigma}\right)^{\frac{1}{2}} I_1\right]\right\}$$

$$= \frac{\pi A_o}{2} - \frac{\pi A_2}{4} + \frac{1}{4}\left(\frac{3C_J}{\sigma}\right)^{\frac{1}{2}}\left[\frac{A_o}{\alpha} I_3 - \alpha I_2 + \frac{C_L}{2\pi} I_4\right] \qquad \ldots(2.32)$$

where the additional integrals I_2, I_3 and I_4 may also be solved in closed form.[33]

$$I_2 = \int_0^{\cos^{-1}(2\lambda-1)} \frac{\cos\Phi_n \sin\Phi_n \, d\Phi_n}{\left(2\cos\Phi_n + 2 - 4\lambda + \frac{S_o}{a}\right)^{1/2}} = \frac{2}{3}\left(1-\lambda+\frac{S_o}{4a}\right)^{\frac{1}{2}}\left(4\lambda-1-\frac{S_o}{a}\right) - \left(\frac{S_o}{a}\right)^{\frac{1}{2}}\left[2\lambda-1-\frac{S_o}{3a}\right] \qquad \ldots(2.33)$$

$$I_3 = \int_0^{\cos^{-1}(2\lambda-1)} \frac{\sin^2\Phi_n \, d\Phi_n}{\left(2\cos\Phi_n + 2 - 4\lambda + \frac{S_o}{a}\right)^{1/2}} = \frac{2I_1}{3}\left(2-4\lambda+\frac{S_o}{a}\right) - \frac{2}{3}\sqrt{\lambda(1-\lambda)\frac{S_o}{a}} + \left[\frac{1}{3}\left(4\lambda-\frac{S_o}{a}\right) F\left(\bar{\theta}, \sqrt{1-\lambda+\frac{S_o}{4a}}\right)\right]_{\bar{\theta}}^{\frac{\pi}{2}} \quad \text{for } 1 > \lambda - \frac{S_o}{4a} > 0 \qquad \ldots(2.34)$$

where F is a standard elliptic integral of the first kind.[34, 35]

$$I_4 = \int_0^{\cos^{-1}(2\lambda-1)} \frac{\sin\Phi_n \, d\Phi_n}{\left(2\cos\Phi_n + 2 - 4\lambda + \frac{S_o}{a}\right)^{1/2}} = 2\left[\left(1-\lambda+\frac{S_o}{4a}\right)^{\frac{1}{2}} - \left(\frac{S_o}{4a}\right)^{\frac{1}{2}}\right] \qquad \ldots(2.35)$$

For convenience the integrals I_2, I_3, and I_4 are also plotted as functions of λ and $\frac{S_o}{4a}$ in Figures 4, 5, and 6.

2.2.4 Comparison between the Two Solutions for a Circular-Arc Aerofoil of Small Camber.

The exact solution for the circular-arc aerofoil has been given in section 2.2.1. These values of C_L and C_{M_o} are now compared with the values obtained from the extended thin aerofoil theory for small α and β.

For a circular-arc aerofoil of small camber.

$$x = 2a\cos\Phi, \quad y = a\beta(1 - \cos 2\Phi)$$

and

$$\frac{dy}{dx} = -2\beta\cos\Phi \qquad \ldots(2.36)$$

Thus equations (2.23) give

$$A_o = \alpha, \quad A_1 = 2\beta, \quad A_2 = A_3 \ldots = A_l = \ldots = 0$$

To order β angles χ_n and Φ_n in Figure 2.2 are related by

$$\begin{aligned} \cos\chi_n &= \cos\Phi_n(1 + \beta\sin\Phi_n) \\ \sin\chi_n &= \sin\Phi_n - \beta\cos^2\Phi_n \end{aligned} \qquad \ldots(2.37)$$

Comparing equations (2.12) and (2.25)

$$(C_L)_{exact} - (C_L)_{thin\ aerofoil} = \frac{1}{2aU_\infty}\sum_1^N Q_n\left(\cot\frac{\chi_n+\beta}{2} - \cot\frac{\Phi_n}{2}\right)$$

$$= -\frac{\beta}{2aU}\sum_1^N Q_n \qquad \text{to order } \beta$$

$$= -\frac{\beta}{2a}\left[\frac{3_a C_J}{4\sigma}\right]^{\frac{1}{2}} \int_{Slot}^{Trailing\ Edge} \frac{dS}{(S+S_o)^{1/2}} \qquad \text{using equation (2.5)}$$

$$= -\frac{\beta}{2}\left[\frac{3C_J}{\sigma}\right]^{\frac{1}{2}} I_4 \qquad \ldots(2.38)$$

Similarly comparing equations (2.15) and (2.31)

$$(C_{M_o})_{exact} - (C_{M_o})_{thin\ aerofoil} = \frac{\beta}{4aU_\infty} \sum_1^N Q_n \left[\frac{1}{2} - \cos^2\Phi_n - \frac{1}{4\pi aU_\infty} \sum_1^N Q_n\right]$$

$$= \frac{\beta}{4}\left[\frac{3C_J}{\sigma}\right]^{\frac{1}{2}} \left\{ \frac{I_4}{2} - \frac{1}{4\pi}\left(\frac{3C_J}{\sigma}\right)^{\frac{1}{2}} I_4^{\,2} - \left(1-\lambda+\frac{S_o}{4a}\right)^{\frac{1}{2}} \left[\frac{16}{15}\left(\lambda-\frac{S_o}{4a}\right)^2 - \frac{4}{5}\left(\lambda-\frac{S_o}{4a}\right)+\frac{7}{30}\right] \right.$$

$$\left. + \left(\frac{S_o}{4a}\right)^{\frac{1}{2}} \left[\frac{16}{15}\left(\frac{S_o}{4a}\right)^2 - \frac{8}{3}\left(\frac{S_o}{4a}\right)\left(\lambda-\frac{1}{2}\right) + 2\left(\lambda-\frac{1}{2}\right)^2\right] \right\} \quad \ldots(2.39)$$

Thin aerofoil theory gives results which differ from the exact solution in a term which involves coupling between camber and sink effect. Such second order terms are of course specifically neglected in any first order thin aerofoil theory by the assumption of small perturbations. It would be possible to develop a second order thin aerofoil theory (specifically replacing equation (2.20) by a more exact expression), however this hardly seems worthwhile without, at the same time, examining both the effect of entrainment downstream and the cross coupling between jet flap effect and sink effect. In any case the errors involved are usually small. For a typical case $\lambda = \frac{3}{4}$, $\frac{S_o}{4a} = 0.01$ and with C_J very large, the error in C_L is only 0.32β and the error in C_{M_o} is 0.64β. These relative errors may be even less when jet-flap effects are added. The use of equations (2.25) and (2.31) is therefore certainly satisfactory in most cases, particularly when one recalls the uncertainty surrounding the choice of the parameter σ.

2.3 The Superposition of Jet Flap Effect.

Spence's first-order theory for jet-flap effect may be added to the present analysis on the assumption that there is no significant cross coupling between the entrainment and the jet-flap effects.

The jet is replaced by a vortex sheet which is assumed to lie on an extension of the aerofoil chord. There is an increase of lift associated with both an increase of circulation round the aerofoil itself, and with the additional circulation round the curved jet sheet downstream. The increase varies with the shape of the camber line. For a flat plate aerofoil with undeflected flap, the increase is

$$\Delta C_L = (0.950\, C_J^{\frac{1}{2}} + 1.377\, C_J)\,\alpha + 3.545\, C_J^{\frac{1}{2}}\,(1 + 0.151\, C_J^{\frac{1}{2}} + 0.139\, C_J)^{\frac{1}{2}}\,\tau \qquad \ldots(2.40)$$

where α is the aerofoil incidence and τ is the angle between the axis of the jet and the flat plate at the trailing edge.[28] A recursion formula for the related increase in moment coefficient is given in reference (4).

$$\Delta C_{M_o} = \frac{1}{2}\,\Delta C_L - (C_J + I_{-1})\,\tau - \sum_{n=o}^{N-1} (A_n\tau + B_n\alpha)\,I_n \qquad \ldots(2.41)$$

where the coefficients A, B and I (which should not be confused with those given in the present paper) are tabulated.

For a flat plate aerofoil with deflected flap the increments of ΔC_L and ΔC_M with flap angle are given in convenient graphical form in reference 27. The entrainment terms in equations (2.29) and (2.32) should be added directly to these values to give the total lift and moment.

The solution for a parabolic-arc camber distribution has been obtained by Hough.[36]

3. COMPARISON WITH EXPERIMENT

3.1 Old Data

The theory is now compared with several sets of experimental data. In some cases the values of the relevant parameters, such as $\frac{S_o}{4a}$ and $\frac{U_1}{U_m}$, are not given and an estimate has had to be made. The reasoning behind the choice of the various parameters is discussed in each of the sections which follow.

Malavard, Poisson-Quinton and Jousserandot[1]

Measurements were made on a symmetrical aerofoil of 22.5% thickness fitted with a 12.5% flap. The lift was noticeably greater when blowing was applied to the upper surface of the flap than when it was applied equally to both sides. The results are reproduced in Figure 7. The increase is partly due to a change in the effective angle of the jet at the trailing edge; the measured value of $\Delta\tau$, being 11^o. The associated increment in lift is calculated using Spence's theory for a symmetrical aerofoil (equation 2.40) and is shown in Figure 7. The remainder of the effect can be attributed to jet entrainment.

For the case of symmetrical blowing on both sides of the flap the entrainment effect will be small. Although the convex curvature of the upper surface tends to increase the entrainment of the jet on that side of the flap, the average velocity ratio $\frac{U_1}{U_m}$ is greater on the upper

surface, which tends to reduce the entrainment. The entrainment effect for symmetrical blowing is therefore neglected.

When blowing is applied only to the upper surface, equation (2.29) may be invoked with $\lambda = 0.875$ and $\frac{S_o}{4a} = 0.02$ (an estimate only). Thus $I_1 = 1.15$ from Figure 3. The average value of σ taking account of the convex curvature of the flow is estimated to be 7.3 (equation 2.6) and effect of the streaming flow is neglected. This gives $\Delta C_{L_{entrainment}} = 0.74\ (C_J)^{\frac{1}{2}}$. The results are shown in Figure 7 and are in good agreement with experiment.

Siestrunck(37)

Results are quoted for an NACA 0012 aerofoil with truncated and bevelled trailing edge over which blowing was applied. At $\alpha = 0$ the lift coefficient noticeably exceeded the value computed from jet-flap theory as presented in reference (37) with $\tau = 57^o$ (Curve A of Figure 8). In an attempt to reduce the discrepancy, the effect of a 5% solid flap was added to the theory (Curve B). It is seen that the revised theory is still appreciably in error for $C_J < 0.5$ and indeed it is apparent that most of the discrepancy is due to the neglect of entrainment. Taking account of the convex curvature of the jet (equation 2.6) and accounting for the effect of streaming flow by choosing an average value

of $\frac{U_1}{U_m} = 0.2$, (Figure 2) a value of $\sigma = 7.9$ is chosen. An estimated value of $\frac{S_o}{4a}$ is 0.01 and $\lambda \approx 0.85$. Thus equation (2.29) gives $\Delta C_{L_{entrainment}} = 0.8\ C_J^{\frac{1}{2}}$. This is added to Curve A, and is shown as Curve C. The entrainment theory clearly exhibits the right trend, and is thought to be too low because the quoted values of C_J correspond to values at the trailing edge rather than those at the slot.

Poisson-Quinton(38)

Blowing was applied to a 13% symmetrical aerofoil at $\lambda = 0.75$ and with slot widths ranging from 0.083% to 0.17% chord. Since the jet is straight there is no effect of jet curvature in this case. The value of $\frac{U_1}{U_m}$ is estimated to be less than 0.25 and thus the value of σ may range from 12 to 15. Thus $0.0066 < \frac{S_o}{4a} < 0.017$ giving $I_1 \approx 1.3$. The theoretical curves for the two values of σ are compared with the measurements at $\alpha = 0$ in Figure 9 and are in good agreement. At $\alpha = 5^o$ and 10^o Spence's jet flap theory (equation 2.41) has been added to the entrainment theory. The experimental values of C_L are seen to lie progressively below the theoretical values for increasing α at low C_J. This can be attributed to the loss of effective jet momentum required to energize the boundary layer and overcome the adverse pressure gradient. The agreement at high values of C_J is however quite satisfactory.

With a 25% flap deflected at 15° on the same aerofoil ($\alpha = 0°$) the agreement is much worse (Figure 10) and this is no doubt due mainly to the failure of jet-flap theory. Presumably the jet momentum at the trailing edge is much less than that emanating from the slot and apparently this momentum was not measured. In such cases simple jet-flap theory overestimates the lift and there is then little point in adding the new entrainment theory. This conclusion changes of course if the jet momentum at the trailing edge is either measured or estimated with sufficient accuracy.

Thomas[29]

Blowing was applied to the upper surface of a flap on a symmetrical aerofoil at $\lambda = 0.75$ using a slot width $\frac{b}{4a} = 0.0017$. $\frac{U_1}{U_m}$ is estimated to vary from about 0.2 to 0.5 and an average value of $\sigma = 17$ is chosen (Figure 2). Hence $\frac{S_o}{4a} = 0.019$ giving $I_1 = 1.22$ from Figure 3 and ΔC_L due to entrainment $= 0.512\ C_J^{\frac{1}{2}}$. At a negative incidence $\alpha = -5°$ the negative contribution from flat plate jet flap theory is $-\Delta C_L = 0.083\ C_J^{\frac{1}{2}} + 0.12\ C_J$. The nett increase of lift coefficient is plotted in the lower half of Figure 11 and the agreement with the experimental results is very satisfactory.

With 25% flap deflected downwards through 15° the experimental results are seen to be appreciably below the theoretical prediction as in the previous case for a

deflected flap. Once again this is attributed to the significant amount of jet momentum which is lost in overcoming the adverse pressure gradient over the flap. Although boundary layer separation is prevented[29] when $C_J = 0.01$, it requires an additional C_J of 0.15 to produce the ideal lift of thin aerofoil theory. Although conventional jet flap theory[27] gives less absolute error at large values of C_J, the shape of the experimental results more closely resembles that of the modified theory, indicating that satisfactory agreement might have been obtained if the actual values of C_J and τ at the trailing edge had been used in applying the jet-flap theory.

3.2 New Data

Streamlines for a flat plate aerofoil

The streamlines have been calculated for a flat plate aerofoil at $\alpha = 0^o$ with blowing over the upper surface. These were obtained by separating the real and imaginary parts of complex potential $W(z)$ (Section 2.21 with $\beta = 0$) and adjusting the constant so that $\psi = 0$ on the aerofoil. The resulting equation is similar to that given by Mandl[39]

$$\psi = U_\infty\left(r - \frac{1}{r}\right)\sin\Phi + \left(\frac{1}{2\pi}\sum_1^N Q_n \cot\frac{\Phi_n}{2}\right)\ln r + \frac{1}{2\pi}\sum_1^N Q_n(\Phi - \Phi_n - \pi)$$

$$- \frac{1}{\pi}\sum_1^N Q_n \tan^{-1}\left[\frac{r\sin(\Phi-\Phi_n)}{r\cos(\Phi-\Phi_n)-a}\right]$$

where the principal value of $\tan^{-1}$ is taken and r, Φ are polar coordinates in the circle plane.

The specific case for $\lambda = 0.5$ and $C_J = 0.5$ was calculated using a digital computer and is superimposed on a photograph of the streamlines flowing over such an aerofoil which were taken in a smoke tunnel (Figure 1). The correct amount of blowing was obtained in the model test by matching the position of the leading-edge stagnation point. Despite the existence of a small leading edge separation bubble the agreement is satisfactory, except close to the wake, where the jet entrains air symmetrically on both sides.

Measurements have also been made on a 5% aerofoil of triangular section (i.e. with sharp leading and trailing edges). Blowing was applied to the upper surface at the mid-chord point through a slot of thickness 0.06% chord. A description of these experiments is given in the Appendix. The values of $\frac{U_1}{U_m}$ were measured and varied from 0.2 at the slot to 0.7 at the trailing edge. From Figure 2 σ ranges from 15 to 26. Thus $\frac{S_o}{4a} = 0.01$ and with $\lambda = 0.5$ this gives $I_1 \approx 1.25$. For this shape of aerofoil equations (2.23) give $A_o = \alpha$, $A_1 = 0.2/\pi$, $A_2 = 0$. Since the camber line is inclined at only 2.9^o to the chord line, jet flap effects at zero incidence are negligible.

The measured values of C_L at $\alpha = 0^o$ are compared with the theoretical values and the curve for $\sigma = 22$ is seen to fit the results very well. (Figure 12). It should

be noted that the measurements exhibit an insensitivity to jet pressure ratio, which confirms that the mean value of σ is usually insensitive to compressibility. The nose-up pitching moment is shown in Figure 13. The experimental results exhibit some scatter due to some uncertainty in the graphical integration of the measured pressure distribution. However the results are seen to lie consistently below the theoretical values even at $C_J = 0$, although the slope of the experimental line is roughly the same as that of the theory for $\sigma = 22$.

4. DISCUSSION AND CONCLUSIONS

The effect of jet entrainment for a jet blowing over one side of an aerofoil has been analysed by replacing the jet with a suitable distribution of sinks on the surface of the aerofoil. An exact solution has been obtained for a circular-arc aerofoil of small camber and the particular solution for a flat plate has been used to extend conventional thin aerofoil theory. Formulae are presented for lift (equation 2.29) and nose-up pitching moment (equation 2.32) for a thin aerofoil with arbitrary camber and blowing, and it is shown that these solutions only differ from the exact solution for a circular-arc aerofoil, by a small term involving the product of the camber and a function of the jet-momentum coefficient. The lift coefficient is shown to be proportional to the square root of the momentum coefficient and, in this respect, is similar to the first term in conventional jet-flap theory. The conceptional basis of the new theory has been substantiated by computing the streamlines for one case and comparing them with those obtained experimentally in a smoke tunnel.

The theory has been compared with five sets of experimental data. The comparisons have involved the choice of a suitable mean value for the jet growth parameter σ in each case. σ decreases with increasing convex

curvature of the surface (equation 2.6) and increases as the ratio of streaming flow velocity U_1 to maximum jet velocity U_m increases (Figure 2). The effect of compressibility can usually be neglected. The effective origin of the jet may be computed with sufficient accuracy from the equation $S_o = \frac{2}{3} \sigma b$. The appropriate C_J in the entrainment theory is the value emanating from the slot.

The theory is seen as a useful and sometimes a necessary extension of conventional jet flap theory when the jet is blown over one side of the wing or flap. For small incidences and flap angles the combined theories give good agreement with experiment. For moderate-to-large incidences and flap deflections, however, the entrainment correction tends to be masked, at moderate values of C_J, by uncertainties in the appropriate choice of C_J and τ in the application of conventional jet-flap theory. The current French practice of determining these parameters from wind-off measurements seems to lead to the most accurate predictions. It is anticipated that the new entrainment theory will be of greater practical significance in the future when satisfactory analyses have been developed for the growth and loss of momentum for a wall jet in any pressure gradient.

The effect of entrainment is to increase the lift by increasing the effective camber of the aerofoil. For large momentum coefficients the gains obtained by blowing

over even a small flap (say 10% chord) are substantial and enhance the desirability of using a blown flap rather than a trailing edge jet in applications of the jet-flap principle. The sink effect associated with jet entrainment reduces or even eliminates the adverse pressure gradient ahead of the slot and it would be interesting to use the present theory to examine this form of boundary-layer control as a means of increasing the extent of laminar flow over a wing in the cruise condition. This would involve the use of thin slots situated at about 75% chord on both sides of the aerofoil which would presumably be similar to those proposed some years ago by Griffith.

REFERENCES

1. Malavard, L., Poisson-Quinton, Ph., and Jousserandot, P. — Theoretical and Experimental Investigations of Circulation Control. Translated by Berthoff and Hazen. Princeton U., Report No. 358 (1956)

2. Stratford, B.S. — Early Thoughts on the Jet Flap. Aero. Quart., Vol.7, p.45 (1956)

3. Helmbold, H.B. — The Lift of a Blowing Wing in a Parallel Stream. J.A.S., Vol.22, p.341 (1955)

4. Spence, D.A. — The Lift Coefficient of a Jet-Flapped Wing. Proc. Roy. Soc., Series A, Vol.238, P.46 (1956)

5. Legendre, R. — Influence de l'emission d'un jet au bord de fuite d'un profil sur l'ecoulement autour de ce profil. C.R.Acad Sci., Paris (1956)

6. Woods, L.C. — Some Contributions to Jet-Flap Theory and to the Theory of Source Flow from Aerofoils. A.R.C., C.P. No.388 (1958)

7. Malavard, L. — Sur une théorie lineaire du du soufflage au bord de fuite d'un profil d'aile. C.R.Acad Sci., Paris (1956)

8. Taylor, G.I. — Flow Induced by Jets. J.A.S. Vol.25, p.464 (1958)

9. Schlichting, H. — Boundary Layer Theory. 4th ed., McGraw Hill, p.605 (1960)

10. Newman, B.G. — Deflection of Plane Jets by Adjacent Boundaries - Coanda Effect. B.L. and Flow Control, Vol.I, edited by Lachmann, Pergamon Press (1961)

11. Carriere, P. and Eichelbrenner, E.A. — Theory of Flow Reattachment. B.L. and Flow Control. Vol.I, edited by Lachmann, Pergamon Press, p.212 (1961)

12. Reichardt, H. — On a New Theory of Free Turbulence. J. Roy. Aero. Soc., Vol.47, p.167 (1943)

13. Forthmann, E. — Uber Turbulente Strahlausbreitung. Ing. - Arch. Vol.5, p.42 (1934) NACA. TN 789, (1936).

14. Knystautas, R. — The Turbulent Jet From a Series of Holes in Line. McGill Univ. Mech. Eng. Dept., Rep. 62-1 (1962) (to be published in Aero. Quart., 1963)

15. von Glahn, U.H. — Use of the Coanda Effect for Jet Deflection and Vertical Lift with Multiple Flat-Plate and Curved Plate Deflection Surface. NACA., TN 4377, (1958)

16. Libby, P.A. and Ting, L. — Remarks on the Eddy Viscosity in Compressible Mixing Flows. J.A.S. Vol.27, p.797 (1960)

17. Mager, A. — Transformation of the Compressible Turbulent Boundary Layer. J.A.S., Vol.25, p.305 (1958)

18. Pai, S. — Fluid Dynamics of Jets. p.148, Von Nostrand. (1954)

19. Crane, L.J. — The Laminar and Turbulent Mixing of Jets of Compressible Fluid. Part II, The Mixing of Two Semi-Infinite Streams. J.F.M., Vol.3, p.81 (1957)

20. Myers, G.E., Schauer, J.J. and Eustis, R.H. — The Plane Turbulent Wall Jet, Part I. Jet Development and Friction Factor. Dept. of Mech. Eng., Stanford U., Technical Rep. No.1 (June 1961)

21. Schwarz, W.H. and Cosart, W.P. — The Two-Dimensional Turbulent Wall Jet. J.F.M., Vol.10, Part 4, p.481 (June 1961)

22. Patel, R.P. — Self-Preserving Two-Dimensional Turbulent Jets and Wall Jets in a Moving Stream. McGill Univ., M.Eng. thesis (1962)

23. Patel, R.P. and Newman, B.G. — Self-Preserving Two-Dimensional Turbulent Jets and Wall Jets in a Moving Stream. McGill Univ., Mech. Eng. Res. Labs., Rep. Ae.5 (1962)

24. Sawyer, R.A. — Two-Dimensional Turbulent Jets with Adjacent Boundaries. Cambridge Univ., Ph.D. Thesis (1962)

25. Stratford, B.S. Jawor, Z.M. and Golesworthy, G.T. — The Mixing with Ambient Air of a Cold Airstream in a Centrifugal Field. N.G.T.E., Memo No.355 (1962)

26. Fekete, G.I. — Private Communication

27. Spence, D.A. — The Lift on a Thin Aerofoil with a Jet-Augmented Flap. Aero. Quart., Vol.9, p.287 (1958)

28. Spence, D.A. — Simple Results for a Two-Dimensional Jet Flap Aerofoil. Aero. Quart., Vol.9, p.395 (1958)

29. Thomas, F. — Untersuchungen über die Erhöhung des Auftriebes von Tragflügeln mittels Grenzschichtbeeinflussung durch Ausblasen. Z. Flugwiss, Vol.2, No.10, p.46 (1962)

30. Attinello, J.S. — Design and Engineering Features of Flap Blowing Installations. B.L. and Flow Control, Vol.I, edited by Lachmann, Pergamon Press, p.488 (1961)

31. Milne Thomson, L.M. — Theoretical Hydrodynamics. 4th Edition. Macmillan (1960)

32. Glauert, H. — The Elements of Aerofoil and Airscrew Theory. Cambridge Univ. Press. (1926)

33. Grobner, W. and Hofreiter, N. — Integral Tables. Springer - Verlag, p.75 (1961)

34. Jahnke, E. Emde, F. and Lösch, F. — Tables of Higher Functions. 6th Edition, McGraw-Hill (1960)

35. Peirce, B.O. — A Short Table of Integrals. Ginn. (1956)

36. Hough, G.R. — Cambered Jet-Flap Aerofoil Theory. Cornell U., Grad. Sch. Aero. Eng. Rep. (1959)

37. Siestrunck, R. — General Theory of the Jet-Flap in Two-Dimensional Flow. B.L. and Flow Control, Vol.I, edited by Lachmann, Pergamon Press, p.358 (1961)

38. Poisson-Quinton, Ph. — Recherches Theoriques et Experimuntales sur le Controle de la Couche Limite. Seventh International Congress of Applied Mechanics. Vol.II, Part 2, p.365 (1948)

39. Mandl, P. — Effect of Standing Vortex on Flow About Suction Aerofoils with Split Flaps. N.R.C.(Canada), Aero. Rep. LR-239. (1959)

40. Wygnanski, I. and Newman, B.G. — General Description and Calibration of the McGill 3ft x 2 ft. Low Speed Wind Tunnel. McGill Univ. Mech. Eng. Res. Labs., Rep. No. Ae.4 (1961)

APPENDIX

Details of the Experimental Investigation

A 5% thick aerofoil of triangular section and symmetrical fore and aft, was mounted vertically in the McGill 3 ft x 2 ft wind tunnel[40]. Such an aerofoil with sharp leading and trailing edges is typical of that used on supersonic aircraft, and was tested for this reason. The aerofoil chord was 15 ins so that the wind tunnel interference was negligible at small incidences and jet momentum coefficients. Thirty nine static pressure taps (0.013 ins diameter) were distributed over the upper and lower surfaces, and the lift and moment were obtained by graphical integration of the pressure distribution. The blowing slot at 50% chord was 0.009 ins thick ($\frac{b}{4a}$ = 0.06%) and was supplied by high-pressure compressors having a total capacity of 0.3 lb. per second. The mass flow was measured with an orifice meter in the supply pipe using measured values of total temperature and pressure there, and this was checked against calculations using the measured total pressure in the plenum chamber of the wing assuming an isentropic expansion to freestream static pressure when the slot was unchoked.[30] The momentum coefficients were calculated in the same way and are considered to be accurate to $\pm$ 3%. The wind tunnel was run at incompressible speeds (< 150 per second) at chordwise Reynolds numbers of the order of 10^6,

The smoke tunnel tests (Figure 1) were run at $R_e \approx 2 \times 10^4$.

Flow Visualization in a Smoke Tunnel

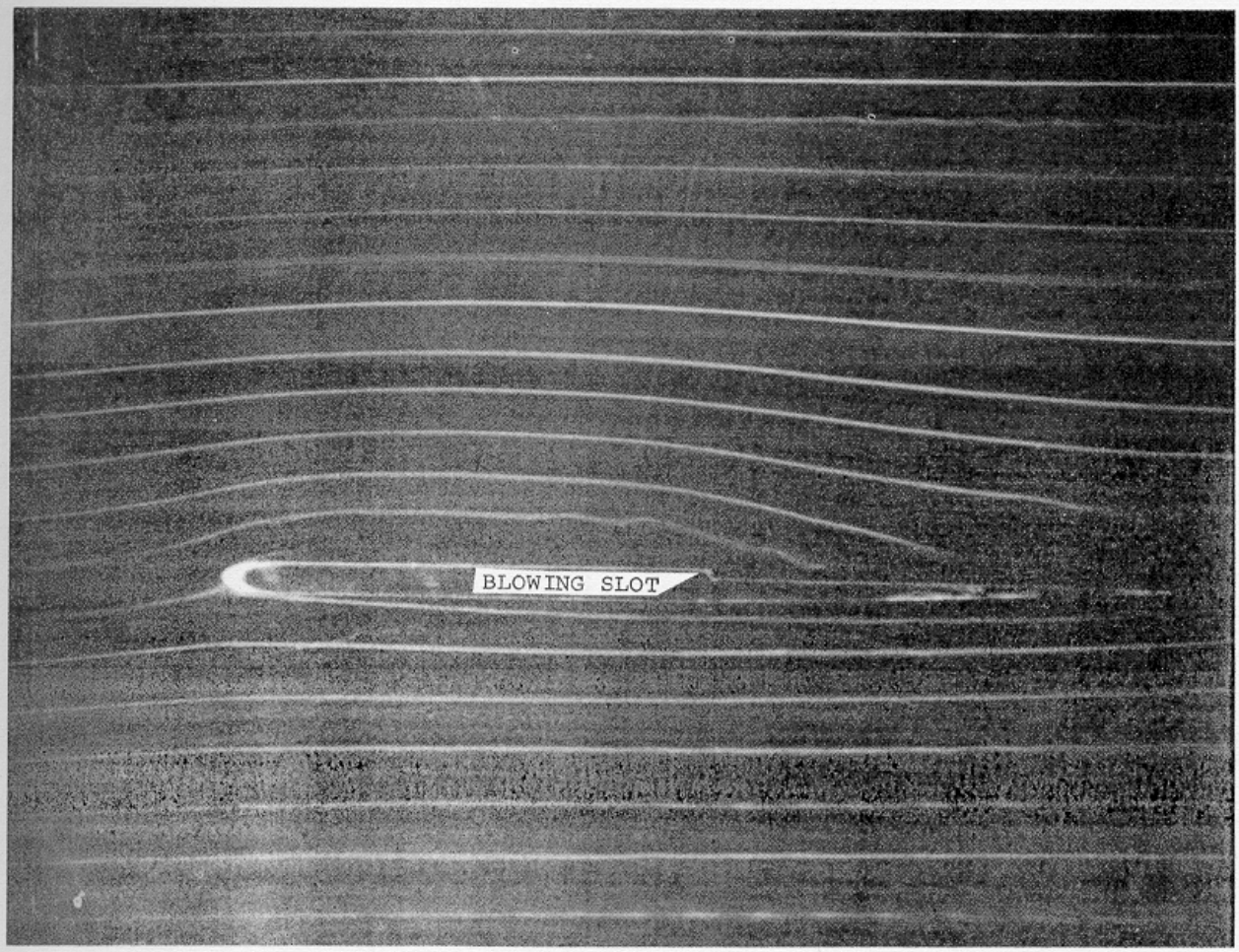

SUPERPOSITION OF COMPUTED STREAMLINES
ON A SMOKE TUNNEL PICTURE
(— — COMPUTED)

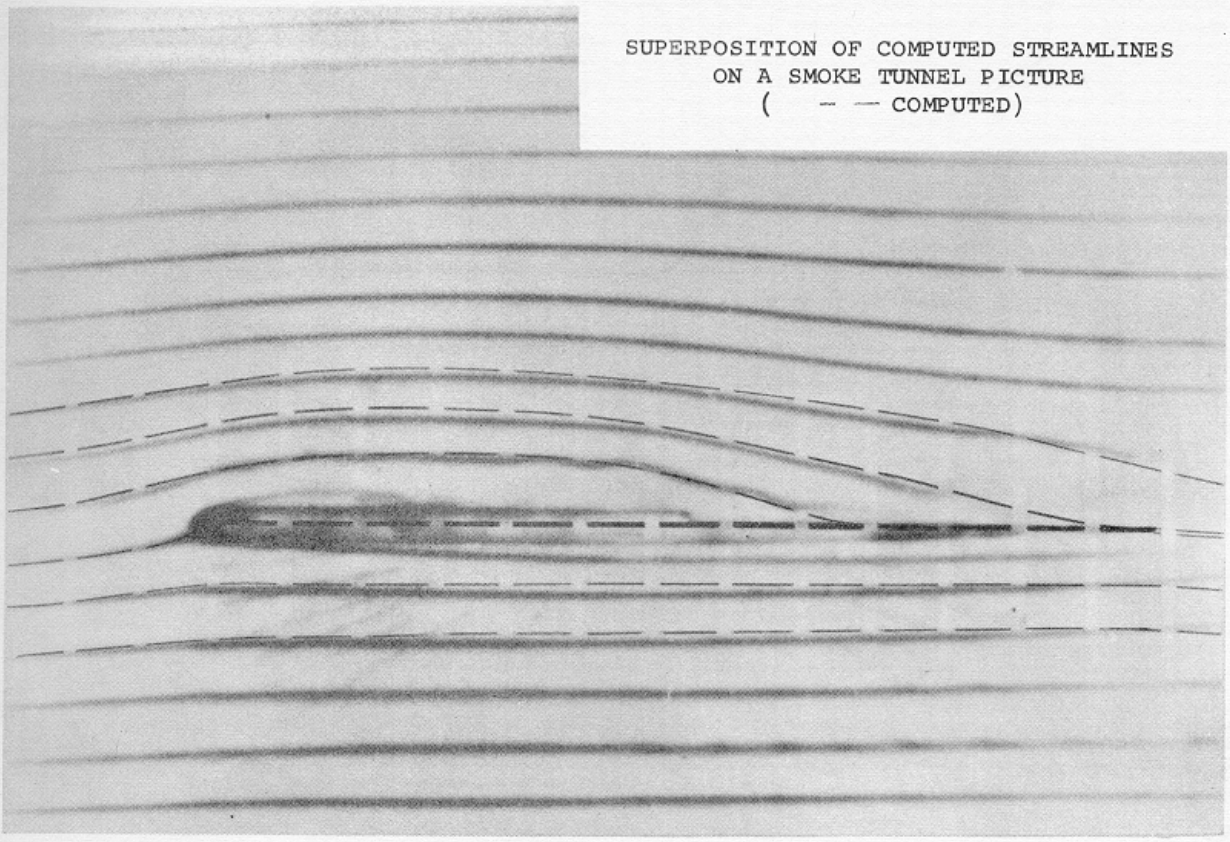

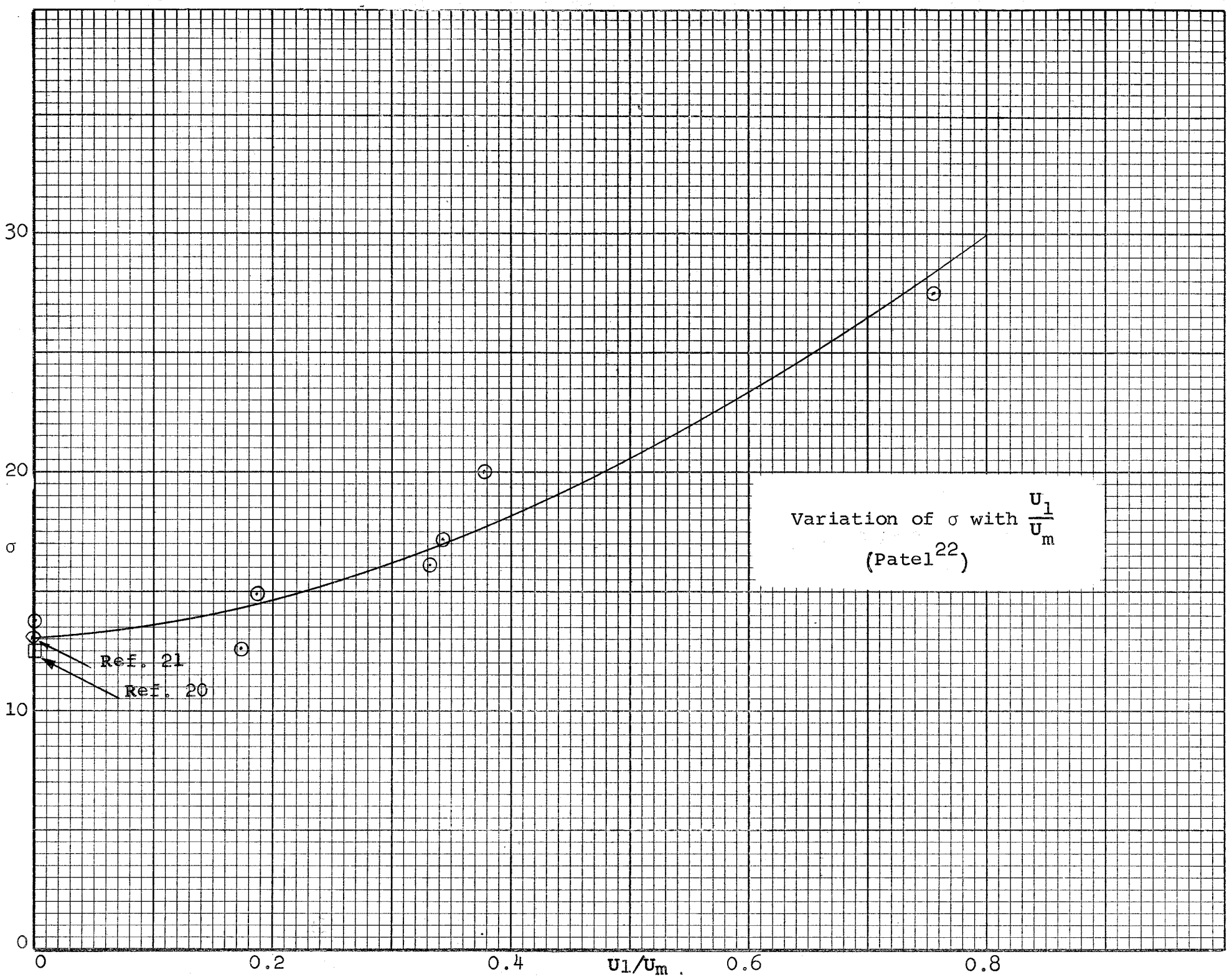
30
20
σ
10
0
0
0.2
0.4
U1/Um
0.6
0.8
Variation of σ with U1/Um
(Patel[22])
Ref. 21
Ref. 20

Figure 2

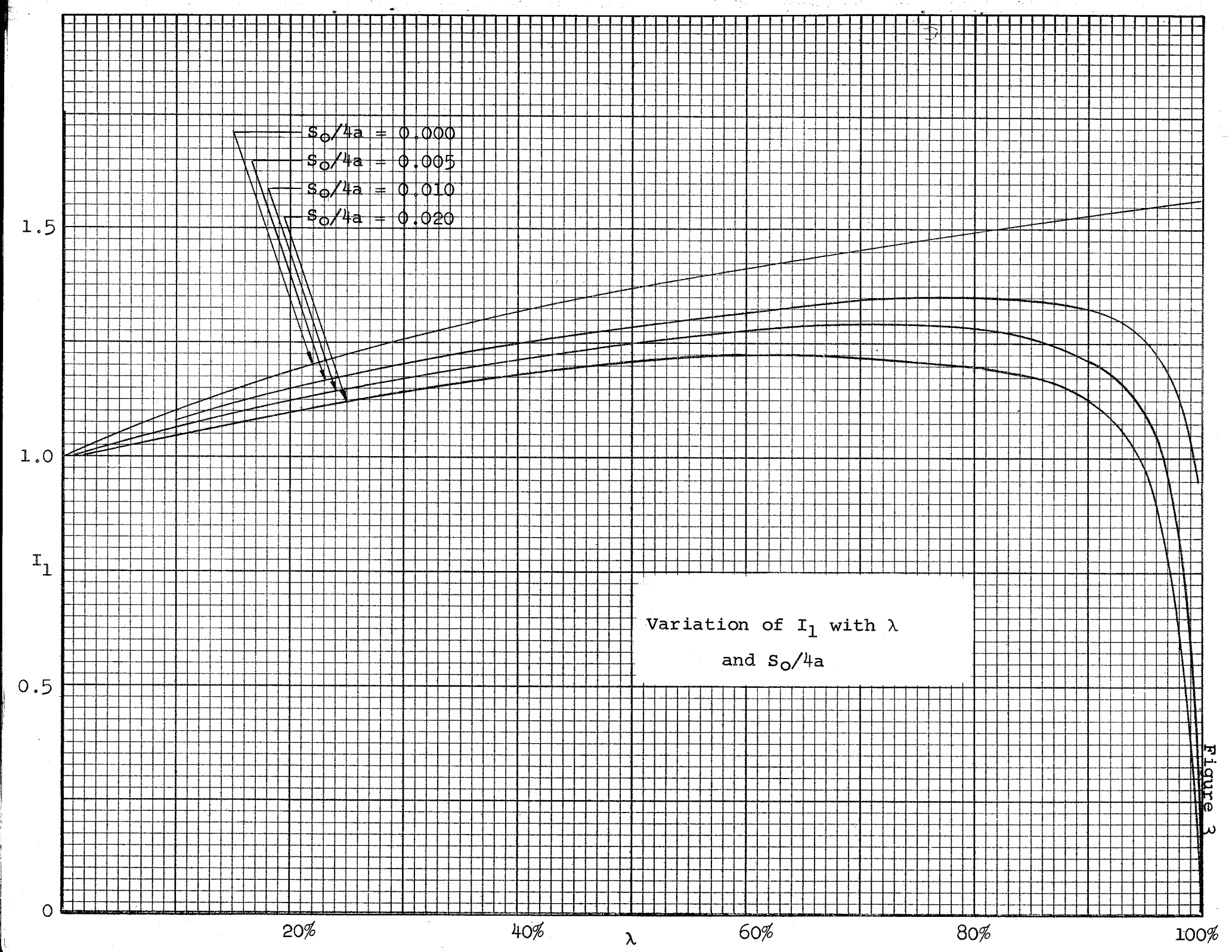
$S_o/4a = 0.000$
$S_o/4a = 0.005$
$S_o/4a = 0.010$
$S_o/4a = 0.020$
1.5
1.0
0.5
0
I_1
20%
40%
60%
80%
100%
λ
Variation of I_1 with λ and $S_o/4a$

Figure 3

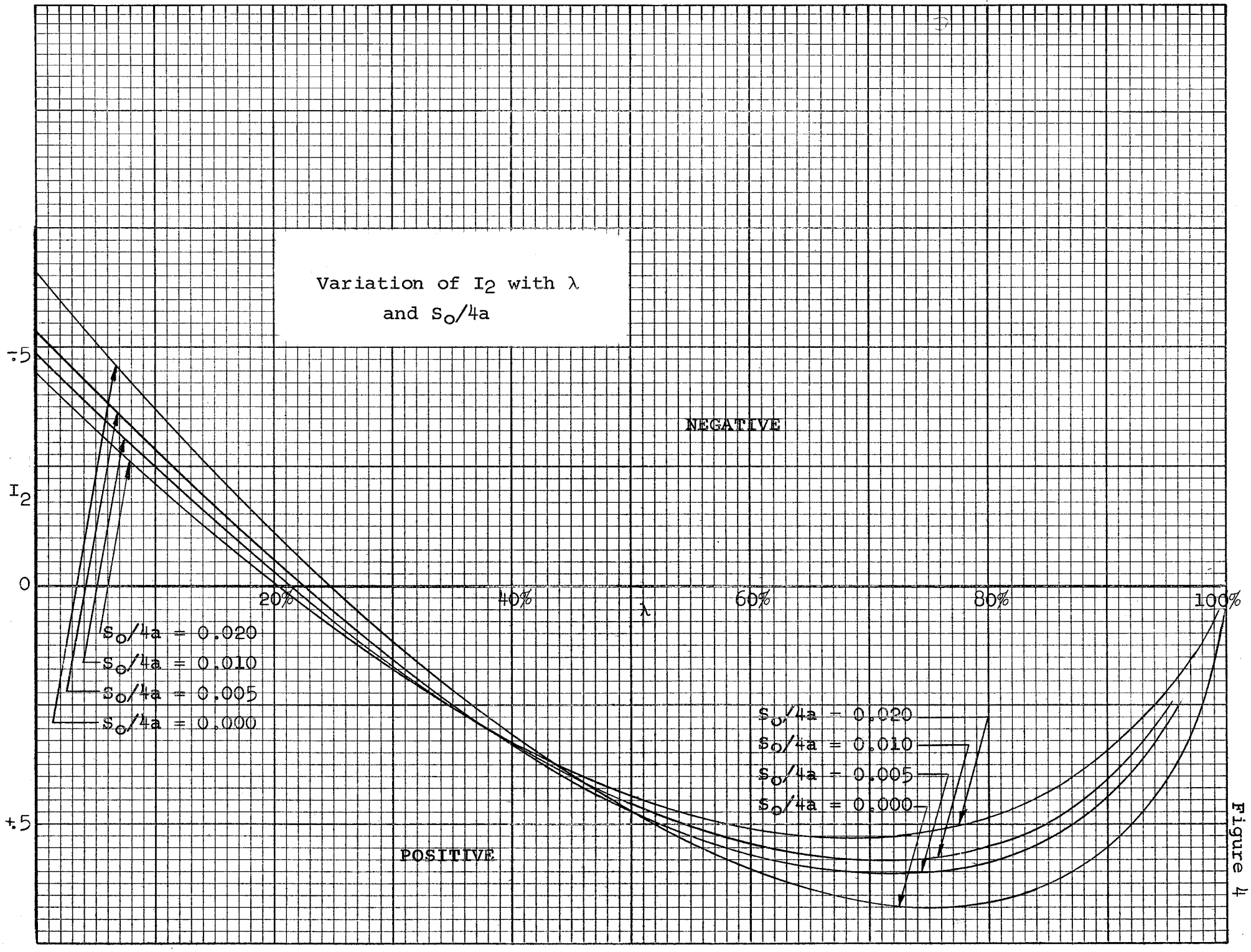
Variation of I_2 with λ
and $S_o/4a$
.5
I_2
0
.5
20%
40%
λ
60%
80%
100%
NEGATIVE
POSITIVE
$S_o/4a$ = 0.020
$S_o/4a$ = 0.010
$S_o/4a$ = 0.005
$S_o/4a$ = 0.000
$S_o/4a$ = 0.020
$S_o/4a$ = 0.010
$S_o/4a$ = 0.005
$S_o/4a$ = 0.000

Figure 4

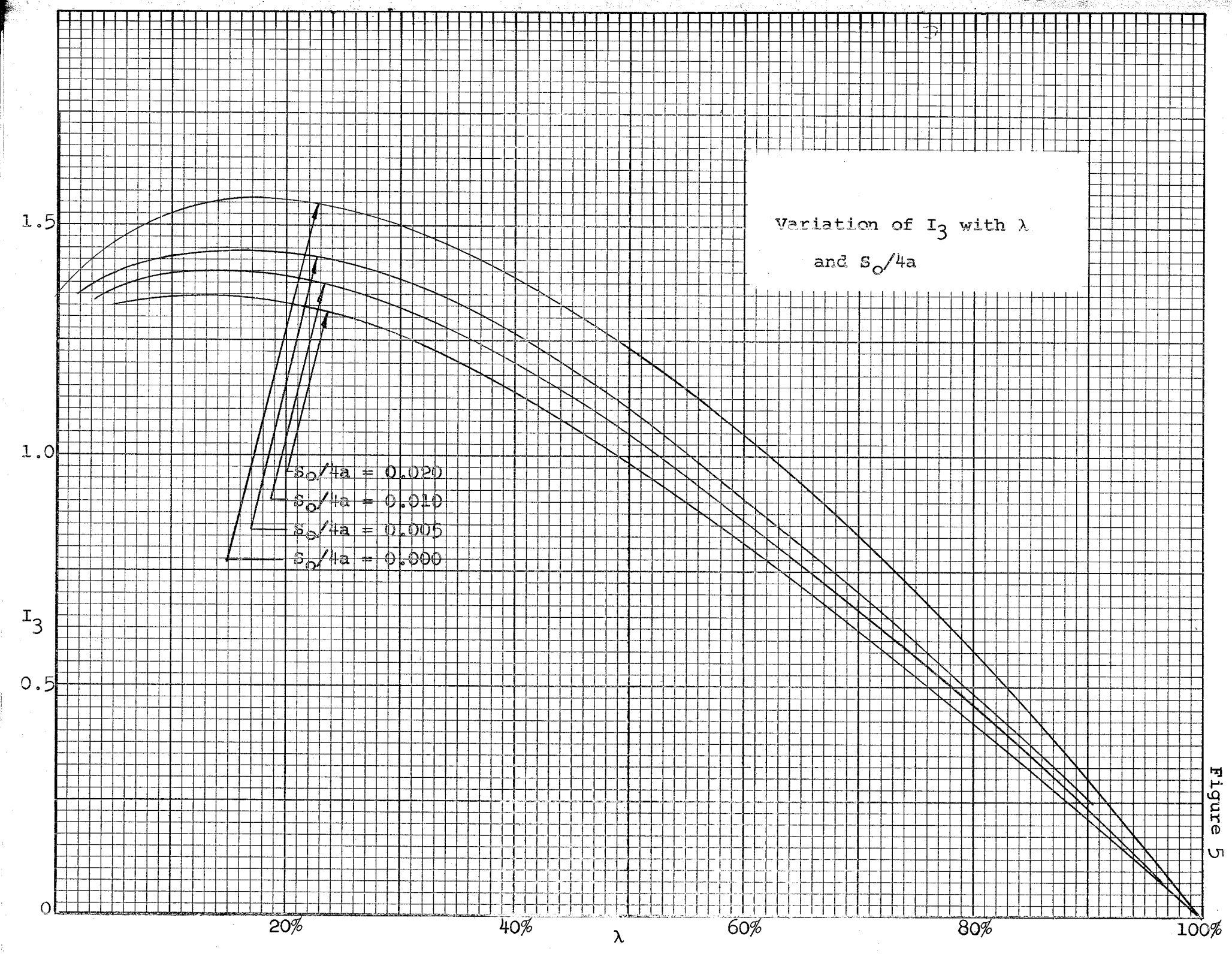
Variation of I_3 with λ and $S_o/4a$
1.5
1.0
0.5
0
I_3
$S_o/4a = 0.020$
$S_o/4a = 0.010$
$S_o/4a = 0.005$
$S_o/4a = 0.000$
20%
40%
60%
80%
100%
λ

Figure 5

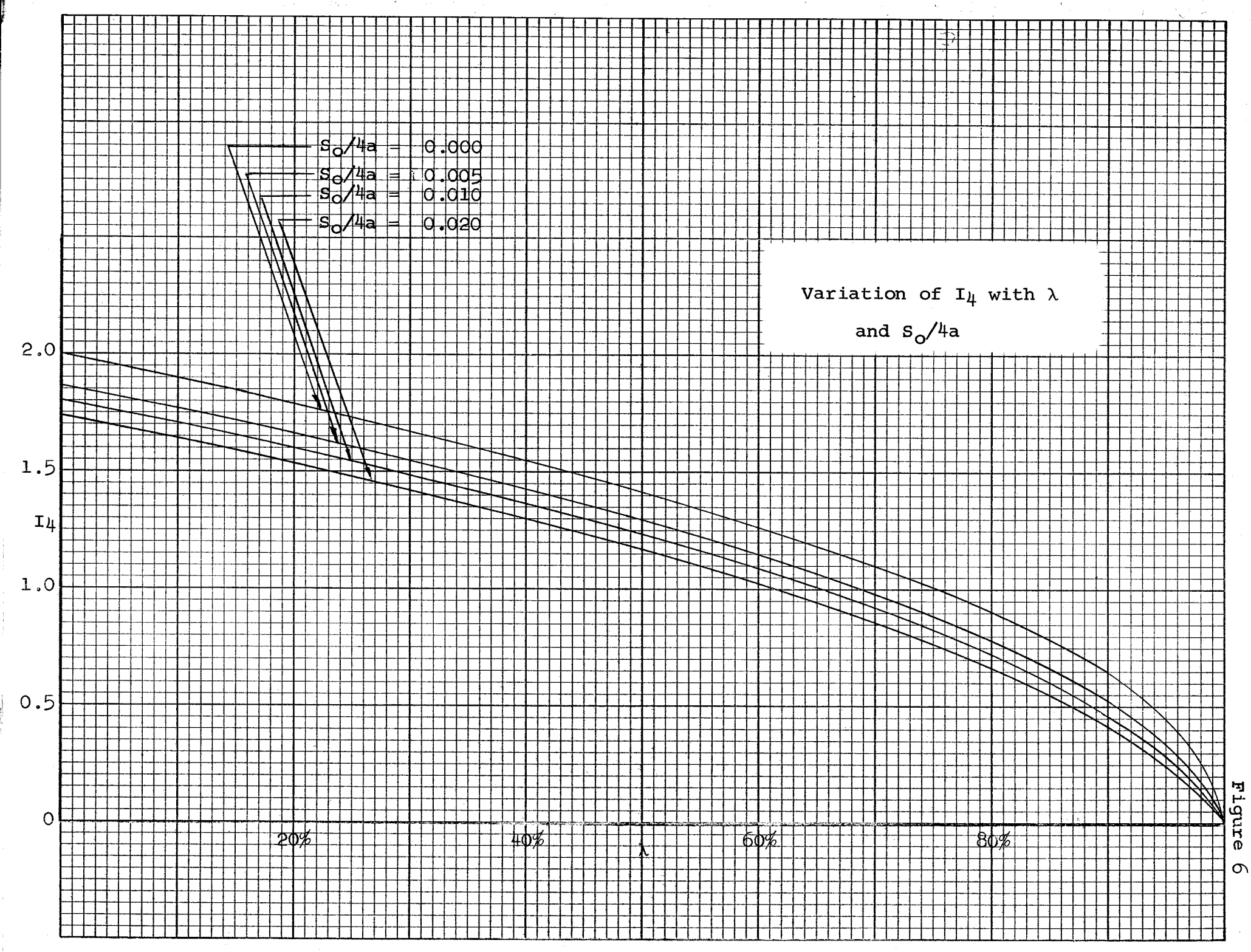
$S_o/4a$ = 0.000
$S_o/4a$ = 0.005
$S_o/4a$ = 0.010
$S_o/4a$ = 0.020
Variation of I_4 with λ
and $S_o/4a$
2.0
1.5
I_4
1.0
0.5
0
20%
40%
λ
60%
80%

Figure 6

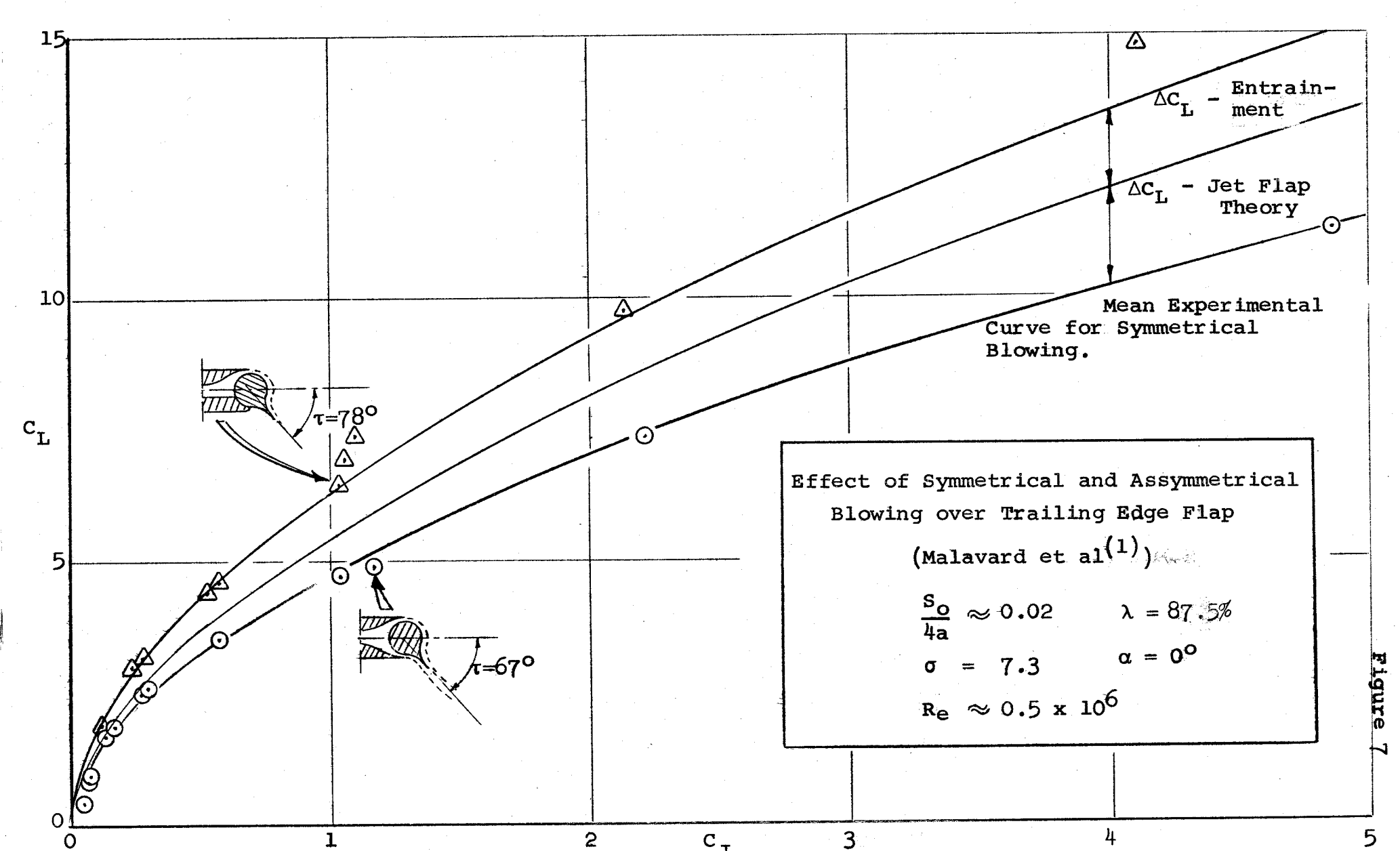
15
10
5
0
0
1
2
3
4
5
C_L
C_J
ΔC_L - Entrain-ment
ΔC_L - Jet Flap Theory
Mean Experimental Curve for Symmetrical Blowing.
τ=78°
τ=67°
Effect of Symmetrical and Assymmetrical Blowing over Trailing Edge Flap
(Malavard et al(1))
$\frac{S_o}{4a} \approx 0.02$
$\lambda = 87.5\%$
$\sigma = 7.3$
$\alpha = 0°$
$R_e \approx 0.5 \times 10^6$

Figure 7

Effect of Blowing over the Upper Surface of a Truncated NACA 0012 Aerofoil.

(Siestrunck[37])

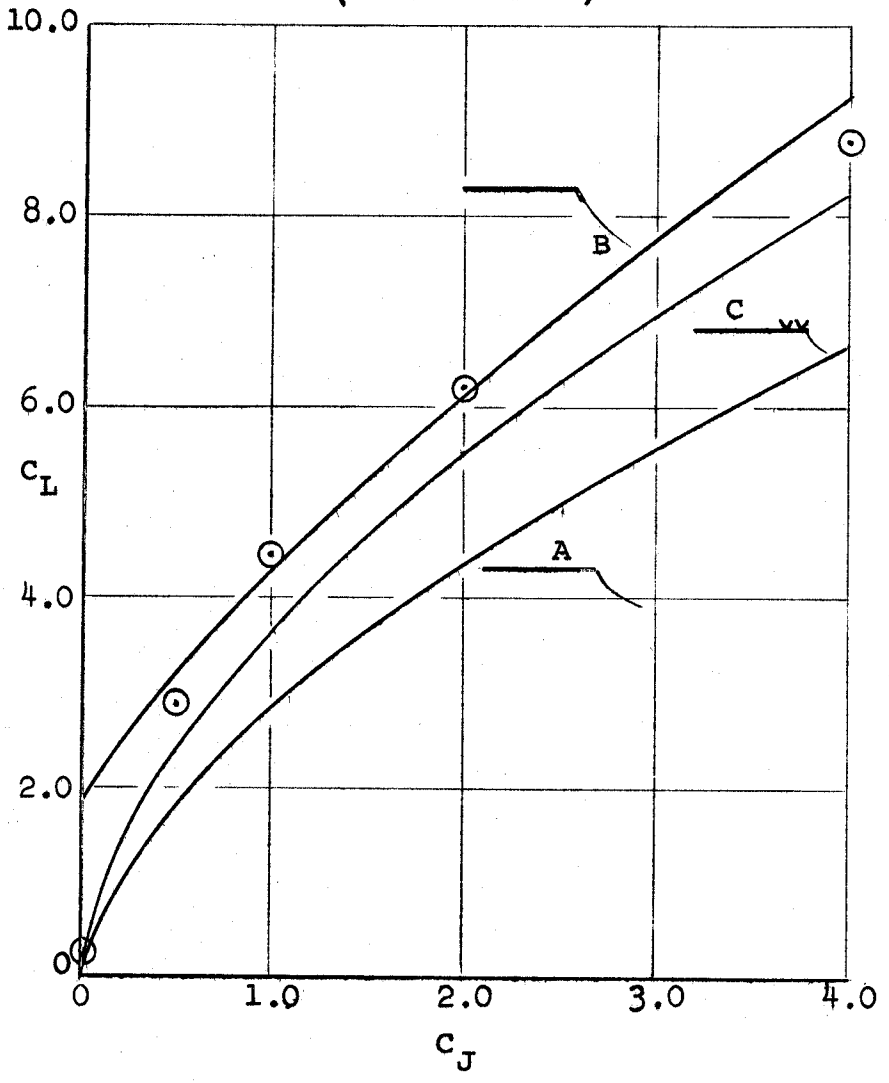

Theoretical Curves

A - Pure Jet Flap

B - Jet Flap + 5% Solid Flap

C - Jet Flap + Entrainment Effect

$\frac{S_o}{4a} \approx .01$ $\lambda \approx .85$

$\sigma \approx 7.9$ $\alpha = 0^\circ$

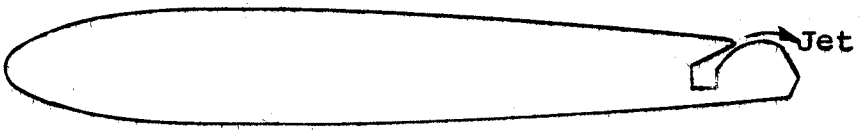

Figure 9

Blowing over the Top of a 13% Symmetrical Aerofoil
(Poisson-Quinton[38])

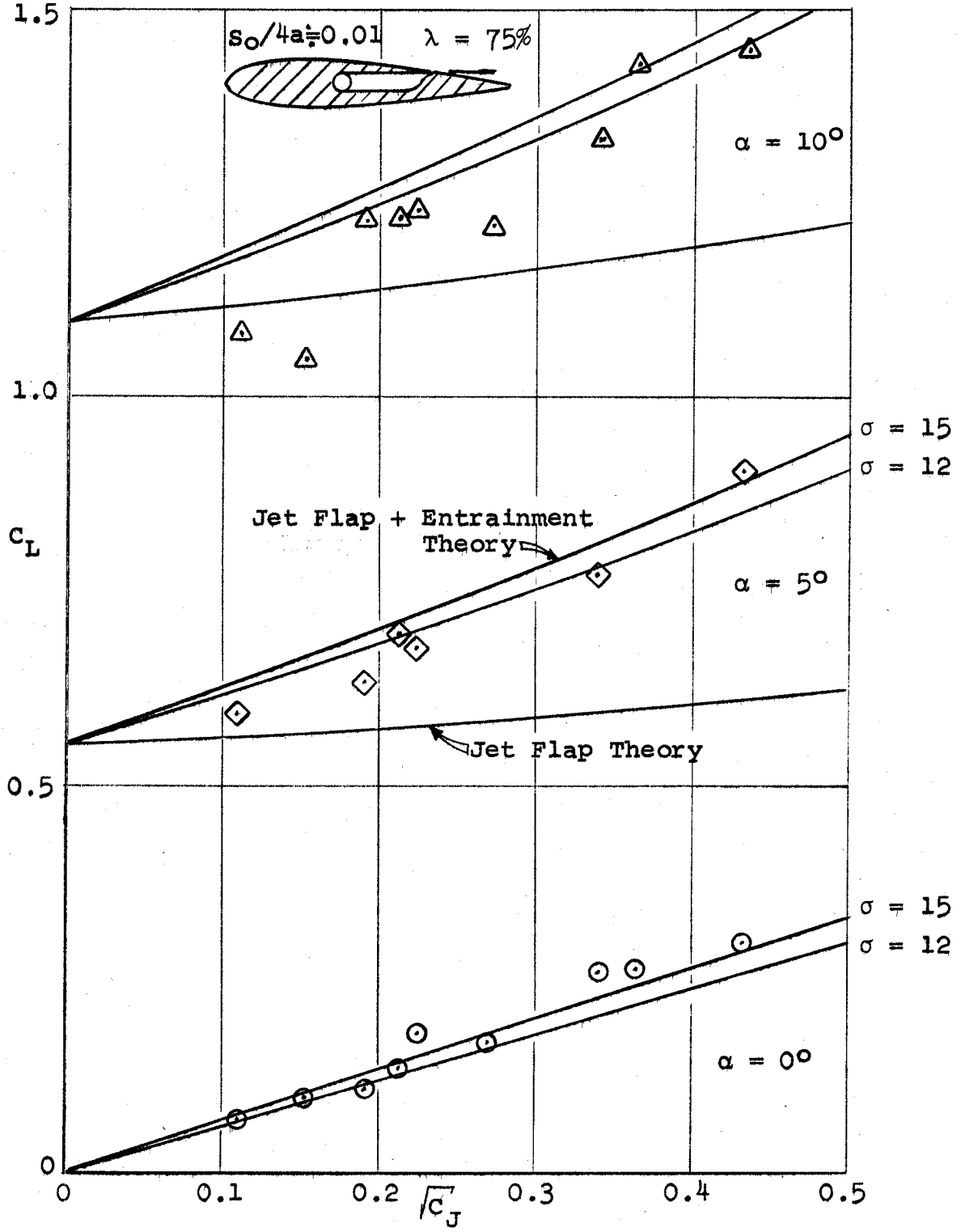

Blowing over the Top of a 13% Symmetrical Aerofoil
(Poisson-Quinton[38])

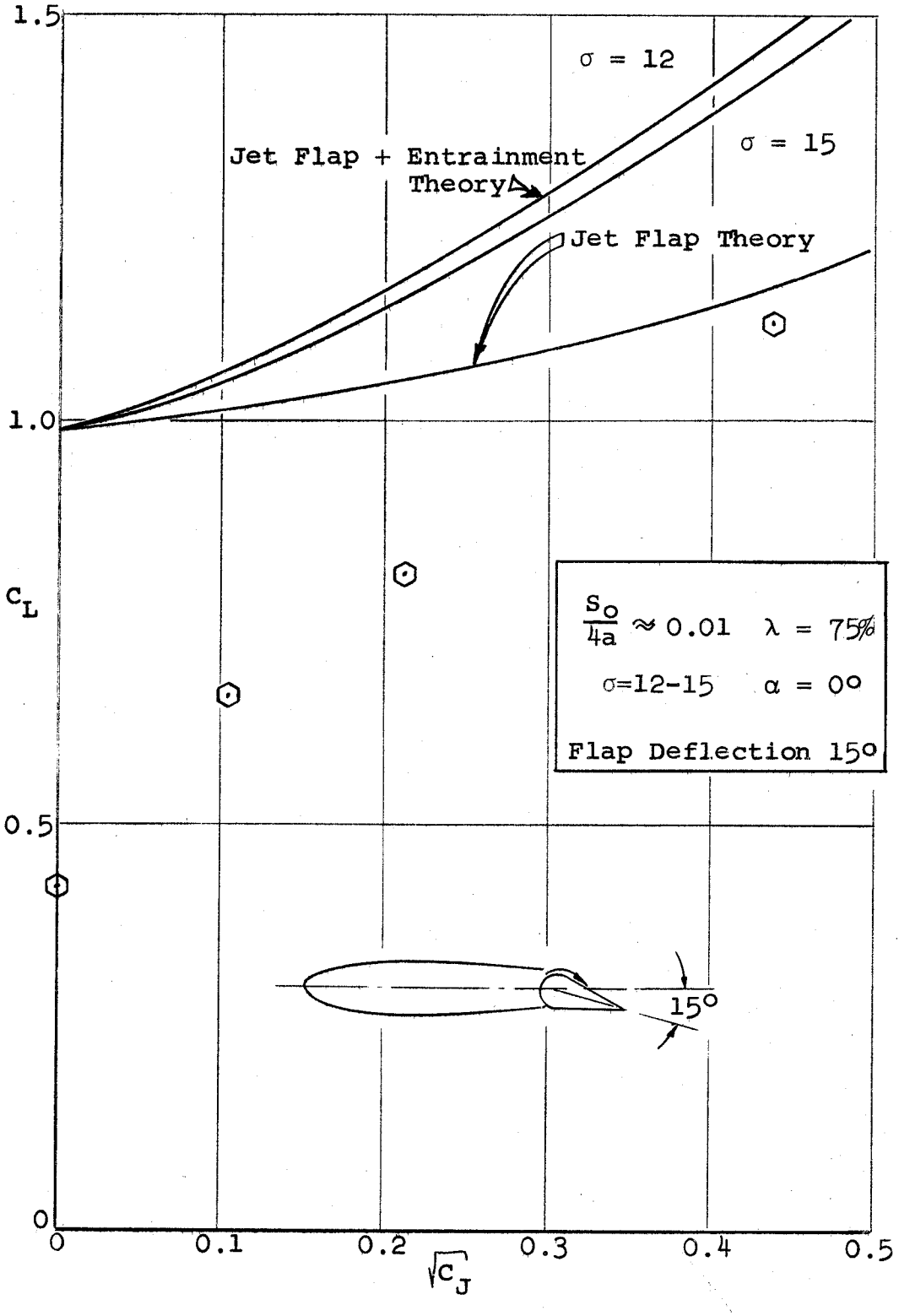

Figure 11

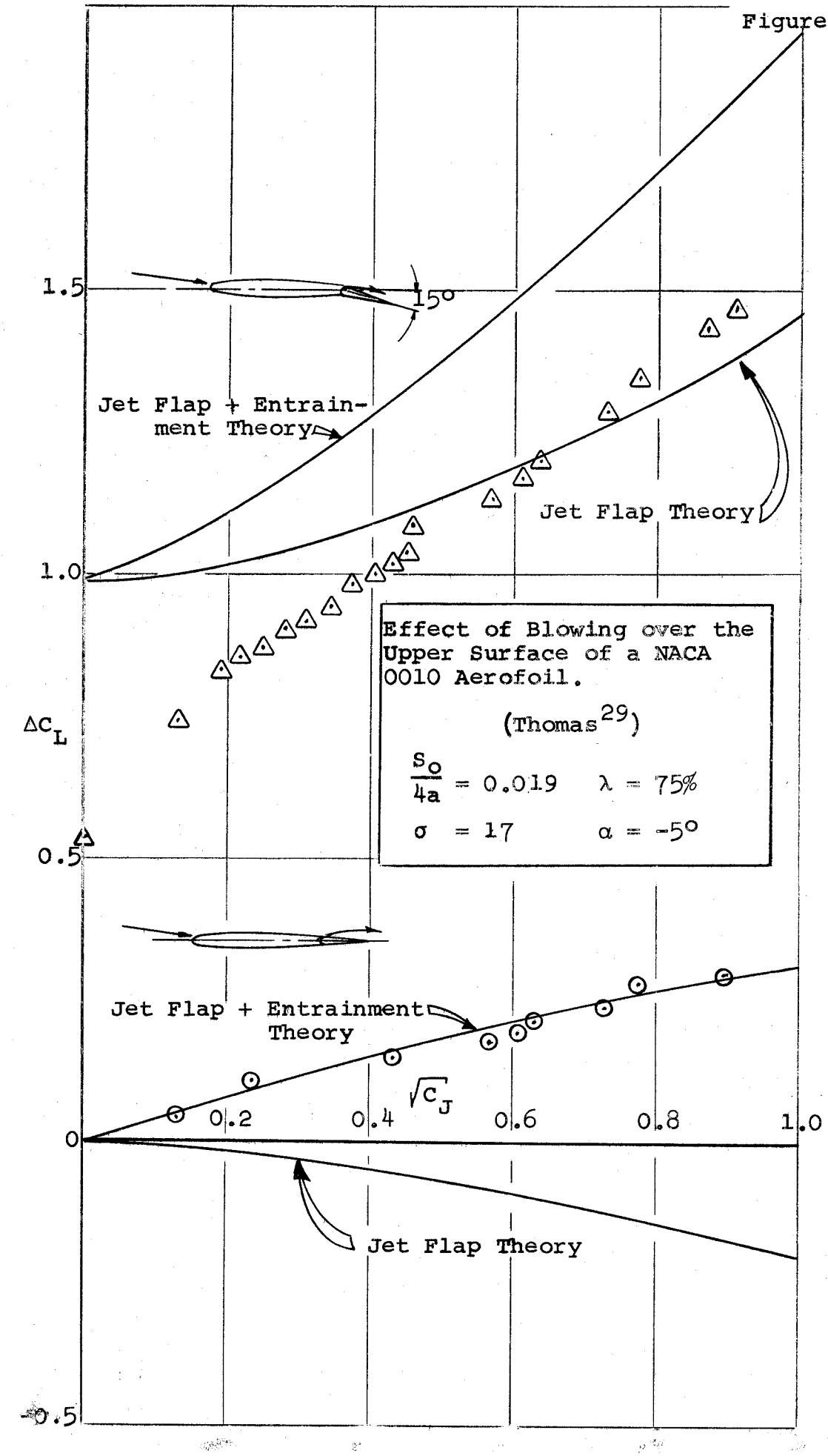
1.5
1.0
0.5
0
-0.5
ΔC_L
15°
Jet Flap + Entrainment Theory
Jet Flap Theory
Effect of Blowing over the Upper Surface of a NACA 0010 Aerofoil.
(Thomas 29)
$\frac{S_o}{4a} = 0.019$ $\lambda = 75\%$
$\sigma = 17$ $\alpha = -5°$
Jet Flap + Entrainment Theory
$\sqrt{C_J}$
0.2
0.4
0.6
0.8
1.0
Jet Flap Theory

Blowing over the Upper Surface of a 5% Triangular Aerofoil. Lift at $\alpha = 0^{\circ}$

(Wygnanski)

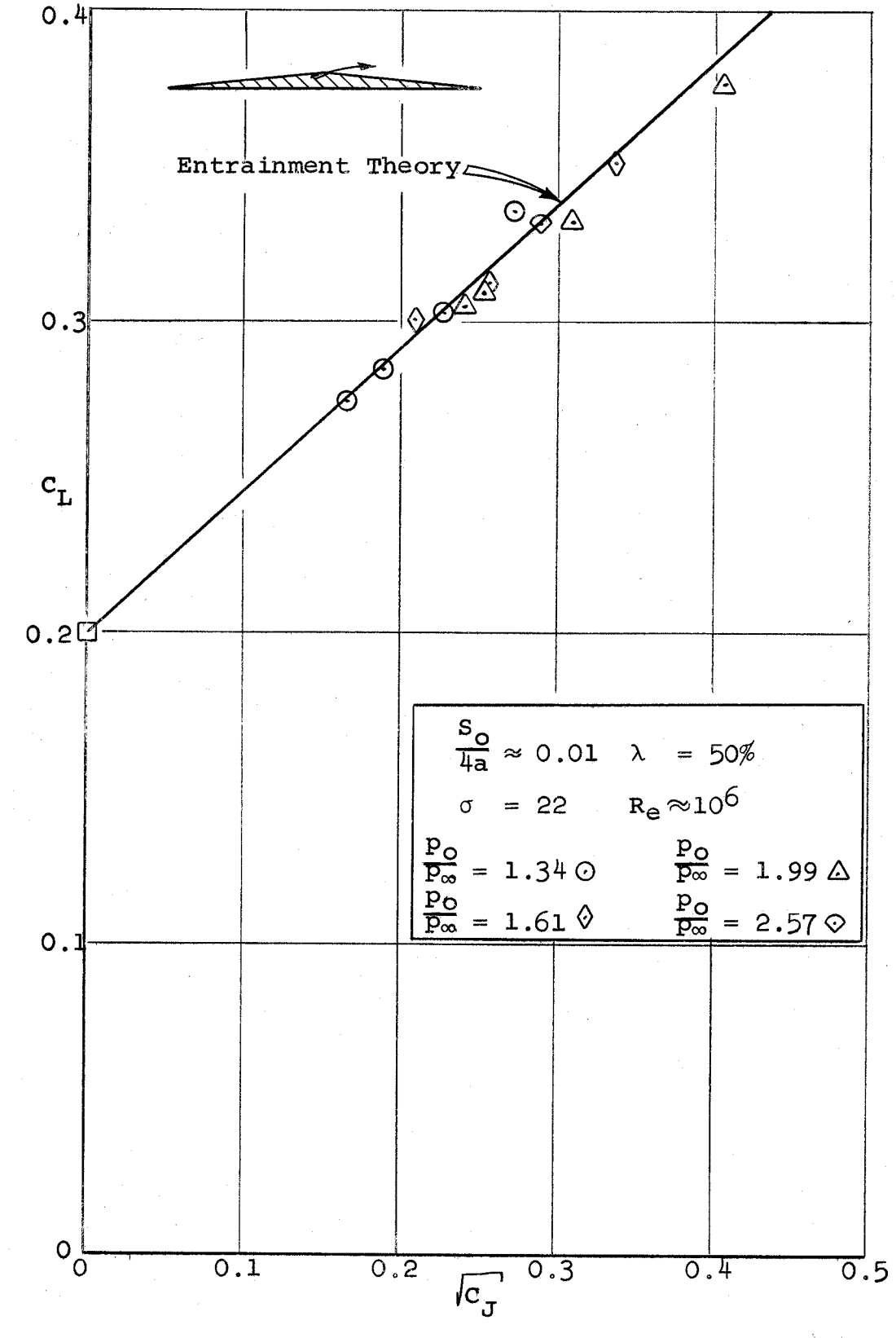

Blowing over the Upper Surface of a 5% Triangular Aerofoil.
Nose up pitching Moment about half chord at $\alpha = 0^{\circ}$
(Wygnanski)